CHAPTER ONE

The Electrodynamics of Left-Handed Media

1.1 INTRODUCTION

Continuous media with negative parameters, that is, media with negative dielectric constant, ε, or magnetic permeability, μ, have long been known in electromagnetic theory. In fact, the Drude–Lorentz model (which is applicable to most materials) predicts regions of negative ε or μ just above each resonance, provided losses are small enough [1]. Although losses usually prevent the onset of this property in common dielectrics, media with negative ε can be found in nature. The best-known examples are low-loss plasmas, and metals and semiconductors at optical and infrared frequencies (sometimes called *solid-state plasmas*). Media with negative μ are less common in nature due to the weak magnetic interactions in most solid-state materials [2]. Only in ferrimagnetic materials are magnetic interactions strong enough (and losses small enough) to produce regions of negative magnetic permeability. Ferrites magnetized to saturation present a tensor magnetic permeability with negative elements near the ferrimagnetic resonance (which usually occurs at microwave frequencies). These materials are widely used in microwave engineering, mainly to make use of their nonreciprocity. The electrodynamics of these solid-state materials with negative ε or μ is described in many well-known textbooks [3–5], so this chapter will focus on the electrodynamics of media having *simultaneously* negative ε and μ (see, however, problems 1.1–1.3, 1.12, and 1.14).

Wave propagation in media with simultaneously negative ε and μ was discussed and analyzed in a seminal paper by Veselago [6] at the end of the 1960s. However, it was necessary to wait for more than 30 years to see the first practical realization of

Metamaterials with Negative Parameters. By Ricardo Marqués, Ferran Martín, and Mario Sorolla

such media [7], also called *left-handed* media [6,7]. This terminology will be used throughout this book.[1] Other terms that have been proposed for media with simultaneously negative ε and μ are *negative-refractive* media [8], *backward* media [9], *double-negative* media [10], and also *Veselago* media [11].

The propagation constant of a plane wave is given by $k = \omega\sqrt{\varepsilon\mu}$, so it is apparent that wave propagation is not forbidden in left-handed media. Several principal questions arise from this statement:

- Does an electromagnetic wave in a left-handed medium differ in any essential way from a wave in an ordinary medium with positive ε and μ?
- Is there any essential physical law—for instance, energy conservation—forbidding left-handed media?
- Assuming the answer to the previous question was affirmative. How to obtain a left-handed medium in practice?

In this chapter we will try to give some answers to the first and second questions above, leaving the following chapters to find the answer to the third question.

1.2 WAVE PROPAGATION IN LEFT-HANDED MEDIA

In order to show wave propagation in left-handed media, we will first reduce Maxwell equations to the wave equation [6]:

$$\left(\nabla^2 - \frac{n^2}{c^2}\frac{\partial^2}{\partial t^2}\right)\psi = 0, \tag{1.1}$$

where n is the refractive index, c is the velocity of light in vacuum, and $n^2/c^2 = \varepsilon\mu$. As the squared refractive index n^2 is not affected by a simultaneous change of sign in ε and μ, it is clear that low-loss left-handed media must be transparent. In view of the above equation, we can obtain the impression that solutions to equation (1.1) will remain unchanged after a simultaneous change of the signs of ε and μ. However, when Maxwell's first-order differential equations are explicitly considered,

$$\nabla \times \mathbf{E} = -j\omega\mu\mathbf{H} \tag{1.2}$$

$$\nabla \times \mathbf{H} = j\omega\varepsilon\mathbf{E}, \tag{1.3}$$

it becomes apparent that these solutions are quite different. In fact, for plane-wave fields of the kind $\mathbf{E} = \mathbf{E}_0 \exp(-j\mathbf{k}\cdot\mathbf{r} + j\omega t)$ and $\mathbf{H} = \mathbf{H}_0 \exp(-j\mathbf{k}\cdot\mathbf{r} + j\omega t)$ (this space and time field dependence will be implicitly assumed throughout this book),

[1]Terms such as *right-* and *left-handed* are of common use in optics, referring to polarized light or to media having optical activity. Therefore, it will be worth noting that the use of the term *left-handed* in this book is not related to any specific polarizing property or structural handedness of the material.

the above equations reduce to

$$\mathbf{k} \times \mathbf{E} = \omega\mu\mathbf{H} \tag{1.4}$$

$$\mathbf{k} \times \mathbf{H} = -\omega\varepsilon\mathbf{E}. \tag{1.5}$$

Therefore, for positive ε and μ, **E**, **H**, and **k** form a right-handed orthogonal system of vectors. However, if $\varepsilon < 0$ and $\mu < 0$, then equations (1.4) and (1.5) can be rewritten as

$$\mathbf{k} \times \mathbf{E} = -\omega|\mu|\mathbf{H} \tag{1.6}$$

$$\mathbf{k} \times \mathbf{H} = \omega|\varepsilon|\mathbf{E}, \tag{1.7}$$

showing that **E**, **H**, and **k** now form a *left-handed* triplet, as illustrated in Figure 1.1. In fact, this result is the original reason for the denomination of negative ε and μ media as "left-handed" media [6].

The main physical implication of the aforementioned analysis is backward-wave propagation (for this reason, the term *backward media* has been also proposed for media with negative ε and μ [9]). In fact, the direction of the time-averaged flux of energy is determined by the real part of the Poynting vector,

$$\mathbf{S} = \frac{1}{2}\mathbf{E} \times \mathbf{H}^*, \tag{1.8}$$

which is unaffected by a simultaneous change of sign of ε and μ. Thus, **E**, **H**, and **S** still form a right-handed triplet in a left-handed medium. Therefore, in such media, energy and wavefronts travel in opposite directions (backward propagation). Backward-wave propagation is a well-known phenomenon that may appear in non-uniform waveguides [12,13]. However, backward-wave propagation in unbounded homogeneous isotropic media seems to be a unique property of left-handed media. As will be shown, most of the surprising unique electromagnetic properties of these media arise from this backward propagation property.

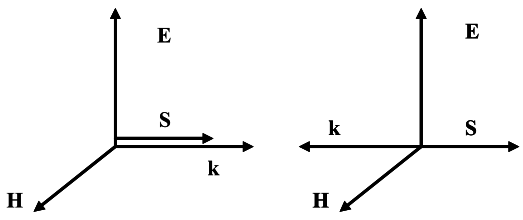

FIGURE 1.1 Illustration of the system of vectors **E**, **H**, **k**, and **S** for a plane transverse electromagnetic (TEM) wave in an ordinary (left) and a left-handed (right) medium.

So far, we have neglected losses. However, losses are unavoidable in any practical material. In the following, the effect of losses in plane-wave propagation will be considered. To begin, we will consider a finite region filled by a homogeneous left-handed medium. In the steady state, and provided there are no sources inside the region, there must be some power flow into the region in order to compensate for losses. Thus, from the well-known complex Poynting theorem [14],

$$\nabla \cdot \{\mathbf{E} \times \mathbf{H}^*\} = \jmath\omega(\mathbf{E} \cdot \mathbf{D}^* - \mathbf{B} \cdot \mathbf{H}^*), \tag{1.9}$$

it follows that

$$\mathrm{Re}\left\{\oint \mathbf{E} \times \mathbf{H}^* \cdot \hat{\mathbf{n}}\, \mathrm{d}S\right\} = \omega\, \mathrm{Im}\left\{\int \left(\mu|\mathbf{H}|^2 - \varepsilon^*|\mathbf{E}|^2\right) \mathrm{d}V\right\} < 0, \tag{1.10}$$

where integration is carried out over the aforementioned region. Therefore,

$$\mathrm{Im}(\varepsilon) < 0; \qquad \mathrm{Im}(\mu) < 0. \tag{1.11}$$

Let us now consider a plane wave with square wavenumber $k^2 = \omega^2\mu\varepsilon$, propagating in a lossy left-handed medium with $\mathrm{Re}(\varepsilon) < 0$ and $\mathrm{Re}(\mu) < 0$. From expression (1.11), it follows that $\mathrm{Im}(k^2) > 0$. Therefore

$$\{\mathrm{Re}(k) > 0 \textit{ and } \mathrm{Im}(k) > 0\} \qquad \textit{or} \qquad \{\mathrm{Re}(k) < 0 \textit{ and } \mathrm{Im}(k) < 0\}. \tag{1.12}$$

That is, waves grow in the direction of propagation of the wavefronts. This fact is in agreement with the aforementioned backward-wave propagation.

1.3 ENERGY DENSITY AND GROUP VELOCITY

If negative values for ε and μ are introduced in the usual expression for the time-averaged density of energy in transparent *nondispersive* media, U_{nd}, given by

$$U_{\mathrm{nd}} = \frac{1}{4}\{\varepsilon|\mathbf{E}|^2 + \mu|\mathbf{H}|^2\}, \tag{1.13}$$

they produce the nonphysical result of a negative density of energy. However, as is well known, any physical media other than vacuum must be dispersive [1], equation (1.13) being an approximation only valid for very weakly dispersive media. The correct expression for a quasimonochromatic wavepacket traveling in a dispersive

media is [2]

$$U = \frac{1}{4}\left\{\frac{\partial(\omega\varepsilon)}{\partial\omega}|\mathbf{E}|^2 + \frac{\partial(\omega\mu)}{\partial\omega}|\mathbf{H}|^2\right\}, \tag{1.14}$$

where the derivatives are evaluated at the central frequency of the wavepacket. Thus, the physical requirement of positive energy density implies that

$$\frac{\partial(\omega\varepsilon)}{\partial\omega} > 0 \qquad \text{and} \qquad \frac{\partial(\omega\mu)}{\partial\omega} > 0, \tag{1.15}$$

which are compatible with $\varepsilon < 0$ and $\mu < 0$ provided $\partial\varepsilon/\partial\omega > |\varepsilon|/\omega$ and $\partial\mu/\partial\omega > |\mu|/\omega$. Therefore, physical left-handed media must be highly dispersive. This fact is in agreement with the low-loss Drude–Lorentz model for ε and μ, which predicts negative values for ε and/or μ in the highly dispersive regions just above the resonances [1]. Finally, it must be mentioned that the usual interpretation of the imaginary part of the complex Poynting theorem, which relates the flux of reactive power through a closed surface with the difference between electric and magnetic energies inside this surface [14], is not applicable to highly dispersive media, where equation (1.14) holds instead of (1.13). Thus, this interpretation is also not valid for left-handed media.

Backward-wave propagation implies opposite signs between phase and group velocities. In fact

$$\frac{\partial k^2}{\partial\omega} = 2k\frac{\partial k}{\partial\omega} \equiv 2\frac{\omega}{v_\mathrm{p}v_\mathrm{g}}, \tag{1.16}$$

where $v_\mathrm{p} = \omega/k$ and $v_\mathrm{g} = \partial\omega/\partial k$ are the phase and group velocities, respectively. In addition, from $k^2 = \omega^2\varepsilon\mu$ and equation (1.15),

$$\frac{\partial k^2}{\partial\omega} = \omega\varepsilon\frac{\partial(\omega\mu)}{\partial\omega} + \omega\mu\frac{\partial(\omega\varepsilon)}{\partial\omega} < 0 \tag{1.17}$$

Finally, from equations (1.16) and (1.17)

$$v_\mathrm{p}v_\mathrm{g} < 0. \tag{1.18}$$

This property implies that wavepackets and wavefronts travel in opposite directions, and can be considered an additional proof of backward-wave propagation in physical left-handed media.

1.4 NEGATIVE REFRACTION

Let us now consider the refraction of an incident optical ray at the interface between ordinary ($\varepsilon > 0$ and $\mu > 0$) and left-handed media. Boundary conditions impose continuity of the tangential components of the wavevector along the interface. Thus, from the aforesaid backward propagation in the left-handed region, it immediately follows that, unlike in ordinary refraction, the angles of incidence and refraction must have opposite signs. This effect is illustrated in Figure 1.2.

From the aforementioned continuity of the tangential components of the wavevectors of the incident and refracted rays, it follows that (Fig. 1.2)

$$\frac{\sin\theta_{\mathrm{i}}}{\sin\theta_{\mathrm{r}}} = \frac{-|\mathbf{k}_2|}{|\mathbf{k}_1|} \equiv \frac{n_2}{n_1} < 0, \tag{1.19}$$

which is the well-known Snell's law. In this expression, n_1 and n_2 are the refractive indices of the ordinary and left-handed media, respectively. Assuming $n_1 > 0$, from equation (1.19) it follows that $n_2 < 0$. That is, the sign of the square root in the refractive index definition must be chosen to be negative [6]:

$$n \equiv -c\sqrt{\varepsilon\mu} < 0. \tag{1.20}$$

For this reason, left-handed media are also referred to as *negative refractive index* or *negative refractive* media.

Geometrical optics of systems containing left-handed media is dominated by this last property. By tracing the paths of optical rays through conventional lenses made of left-handed media, it can be shown that concave lenses become convergent and

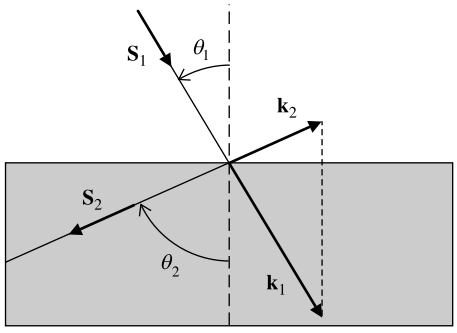

FIGURE 1.2 Graphic demonstration of the negative refraction between ordinary (subscript 1, top) and left-handed (subscript 2, gray area) media. Poynting and wavevectors for each media are labeled as $\mathbf{S}_1$, $\mathbf{S}_2$, $\mathbf{k}_1$, and $\mathbf{k}_2$, respectively. Negative refraction arises from the continuity of the components of the wavevectors, $\mathbf{k}_1$ and $\mathbf{k}_2$, parallel to the interface, and from the fact that rays propagate along the direction of energy flow. That is, they must be parallel to the Poynting vectors $\mathbf{S}_1$ and $\mathbf{S}_2$.

convex lenses become divergent, thus reversing the behavior of lenses made from ordinary media [6]. However, the most interesting effect that can be deduced from the geometrical optics of left-handed media is probably the focusing of energy coming from a point source by a left-handed slab [6]. This effect is illustrated in Figure 1.3. For paraxial rays

$$|n| = \frac{|\sin\theta_1|}{|\sin\theta_2|} \simeq \frac{|\tan\theta_1|}{|\tan\theta_2|} = \frac{a'}{a} = \frac{b'}{b}, \tag{1.21}$$

where n is the refractive index of the left-handed slab relative to the surrounding medium. Therefore, as is illustrated in Figure 1.3, electromagnetic energy coming from the point source is focused at two points, one inside and the other outside the left-handed slab, the latter at a distance

$$x = a + a' + b' + b = d + \frac{d}{|n|} \tag{1.22}$$

from the source, where d is the width of the slab. If $n = -1$ the aforementioned effect is not restricted to paraxial rays, because in this case $|\theta_1| = |\theta_2|$ for any angle of incidence. In fact, when $n = -1$, all rays coming from the source are focused at two points, inside and outside the slab, the latter being at a distance $2d$ from the source. We will return later to this interesting situation.

The above discussion mainly followed the earlier work of Veselago [6]. More recently, negative refraction at the interface between ordinary and left-handed media has been criticized on the basis of the highly dispersive nature of left-handed media [15]. In spite of these criticisms, negative refraction in left-handed media seems now to be well established. In fact, both theoretical calculations [16,17] and experiments [18–22] have confirmed Veselago's predictions. The reader interested in this specific topic can consult the aforementioned references for a more complete discussion.

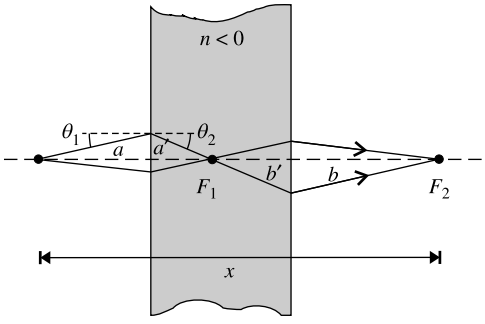

FIGURE 1.3 Graphic illustration of the focusing of paraxial rays coming from a point source by a left-handed slab. Light focuses at two points, F_1 and F_2, inside and outside the slab.

A brief discussion about the meaning and scope of the term *negative refraction* is of interest at this point. In the frame of this section, negative refraction and negative refractive index are equivalent. That is, the incident and refracted beams always lie at the same side of the normal, and Snell's law (1.19) is satisfied with a negative refractive index that does not depend on the angle of incidence. In this *strong* sense, negative refraction seems to be a unique property of isotropic left-handed media. In a less restrictive sense, negative refraction can also be understood as the simple situation where an incident and a refracted beam both lie at the same side of the normal, for a particular angle of incidence. However, it may be worth mentioning that, in this *weak* sense, negative refraction can appear in many physical systems that may not include left-handed media, nor even media with negative parameters. As an illustration of this statement, Figure 1.4 shows the negative refraction of the extraordinary ray at the interface between an ordinary isotropic medium and an hypothetical uniaxial medium with $\varepsilon_\perp > \varepsilon_\parallel$. The isofrequency ellipsoids, $\omega(\mathbf{k}) = \text{constant}$, for the isotropic and the uniaxial media are shown for a specific orientation of the optical axis. For this specific orientation, and for the considered specific angle of incidence, the group velocity $\nabla_k(\omega)$ corresponding to the wavevector of the refracted ray forms a negative angle with the normal (in spite of the fact that the corresponding wavevector $\mathbf{k}_r$ makes a positive angle with the normal). Because the direction of the refracted ray is determined by the group velocity, the refracted ray forms a negative angle with the normal. However, unlike negative refraction in left-handed media, negative refraction in uniaxial media only occurs for very specific orientations of the optical axis, and for very specific angles of incidence and polarizations of the incident light. A more restrictive concept is *all-angle negative refraction* [23]. This means that a negative refraction in the aforementioned *weak* sense is observed for all angles of incidence. All-angle negative refraction, with a refractive index depending on the angle of incidence, has been reported in uniaxial media with negative permittivity or permeability along the optical axis [9] (see problem 1.8). Generalized refraction laws at the interface

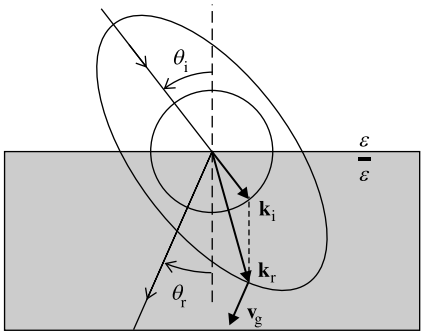

FIGURE 1.4 Graphic demonstration of the negative refraction of the extraordinary ray at the interface between an isotropic and an uniaxial medium. The isofrequency surfaces for both media are shown, and the wavevector and the group velocity of the refracted ray are graphically obtained from these surfaces. The reported negative refraction only occurs for very specific angles of incidence and polarizations.

between anisotropic media with negative parameters are analyzed in detail in [24]. Finally, it may be worth mentioning that negative refraction has been also reported in strongly modulated photonic crystals for some specific frequency bands [25].

1.5 FERMAT PRINCIPLE

As is shown in many textbooks, Snell's law can be deduced from the variational Fermat principle, and vice versa. The variational Fermat principle states that the optical length of the path followed by light between two fixed points, A and B, is an extremum. The optical length is defined as the physical length multiplied by the refractive index of the material. Therefore, the Fermat principle is stated as

$$\delta L = 0, \qquad \text{where} \quad L = \int_{\mathrm{A}}^{\mathrm{B}} n \, \mathrm{d}l. \tag{1.23}$$

Because Snell's law (1.19) still holds for left-handed media, the Fermat principle will also hold for systems containing left-handed media, provided the appropriate definition for n (1.20) is taken in equation (1.23) [8]. It may be worth mentioning that, according to this statement of the Fermat principle, the optical length of the actual path chosen by light is not necessarily a minimum when left-handed media are present. In fact, it may even be negative or null. It also becomes apparent that the time taken by light to travel between two points is not related to the optical length through the usual formula for ordinary weakly dispersive media, that is $t \neq L/c$. Therefore, the path followed by light in optical systems containing left-handed media is not necessarily the shortest in time [8].

From the definition of L (1.23), it follows that the optical length between two points, A and B, on a given optical ray is proportional to the phase advance between such points: $\Delta\phi = -k\overline{AB} = -n(\omega/c)\overline{AB} = -(\omega/c)L$. It is of interest to evaluate the optical length between the source and the focuses, F_1 and F_2, in the experiment shown in Figure 1.3 for the particular case of $n = -1$. It follows immediately that the optical length between the source and the focus is exactly zero for all rays (not only for paraxial rays). Thus, all the rays coming from the source are recovered at the focus with exactly the same phase as at the source. Nevertheless, because the reflection coefficient for each ray depends on the angle of incidence, the intensity of the rays is not reproduced at the focus. However, if $\varepsilon/\varepsilon_0 \to -1$ and $\mu/\mu_0 \to -1$, the wave impedance of the slab becomes equal to that of free space, and the reflection coefficient vanishes for all rays. In such a case, it can be shown that the electromagnetic field at the source is exactly reproduced at the focus [26]. We will return later to this point.

1.6 OTHER EFFECTS IN LEFT-HANDED MEDIA

Backward-wave propagation in left-handed media also has implications in other well-known physical effects related to electromagnetic wave propagation. The following text considers some of them.

1.6.1 Inverse Doppler Effect

When a moving receiver detects the radiation coming from a source at rest in a uniform medium, the detected frequency of the radiation depends on the relative velocity of the emitter and the receiver. This is the well-known Doppler effect. If this relative velocity is much smaller than the velocity of light, a nonrelativistic analysis suffices to describe such an effect. The qualitative analysis is quite simple for ordinary ($n > 0$) media, and can be found in many textbooks. If the receiver moves towards the source, wavefronts and receiver move in opposite directions. Therefore, the frequency seen by the receiver will be higher than the frequency measured by an observer at rest. However, if the medium is a left-handed material, wave propagation is backward, and wavefronts move towards the source. Therefore, both the receiver and the wavefronts move in the same direction, and the frequency measured at the receiver is smaller than the frequency measured by an observer at rest.

A straightforward calculation shows that the aforementioned frequency shifts are given by

$$\Delta\omega = \pm\omega_0 \frac{v}{v_p}, \tag{1.24}$$

where ω_0 is the frequency of the radiation emitted by the source, v is the velocity at which the receiver moves *towards* the source, v_p the phase velocity of light in the medium, and the $\pm$ sign applies to ordinary/left-handed media. Equation (1.24) can be written in a more compact form as [6]

$$\Delta\omega = \omega_0 \frac{nv}{c}, \tag{1.25}$$

where n is the refractive index of the medium and c the velocity of light in free space. In equation (1.25), $\Delta\omega$ is the difference between the frequency detected at the receiver and the frequency of oscillation of the source. For $n < 0$, the frequency shift becomes negative for positive v (receiver moving towards the source), as it was qualitatively shown at the beginning of this section. Interestingly, from equation (1.17), it directly follows that $\mathrm{d}|k|/\mathrm{d}\omega < 0$ in left-handed media. Thus, a negative frequency shift results in an increase of $|k|$. Therefore, a shift towards shorter wavelengths is seen when the receiver approaches the source, both in ordinary and left-handed media.

1.6.2 Backward Cerenkov Radiation

Cerenkov radiation occurs when a charged particle enters an ordinary medium at a velocity higher than the velocity of light in such a medium. If the deceleration of this particle is not too high, its velocity can be considered approximately constant over many wave periods. Then, as is illustrated in Figure 1.5*a*, the spherical wavefronts radiated by this particle become *delayed* with regard to the particle motion,

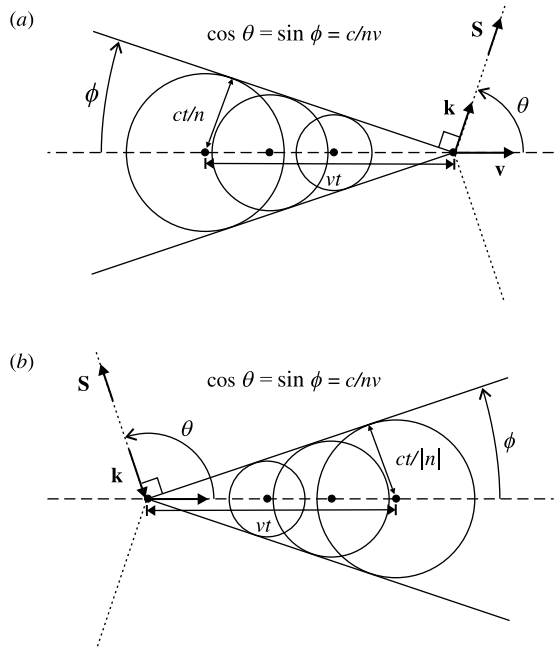

FIGURE 1.5 Illustration of the formation of Cerenkov shock waves: (*a*) in an ordinary medium, and (*b*) in a left-handed medium. In (*a*) the spherical wavefronts move outwards from the source at a velocity c/n. In (*b*) the spherical wavefronts move inwards to the source at a velocity $c/|n|$.

thus giving rise to a *shock wave* [1], which travels forward, making an angle θ with the particle velocity. This angle is given by

$$\cos\theta = \frac{c}{nv}, \tag{1.26}$$

where c/n is the velocity of light in the medium and v the velocity of the particle.

If the medium has a negative refractive index, wave propagation is backward, and the spherical wavefronts corresponding to each frequency harmonic of the radiation move inwards to the source, at a velocity $c/|n(\omega)|$. Therefore, each wavefront collapses at the advanced position of the particle shown in Figure 1.5*b*. Thus, the resulting shock wave travels backward at an obtuse angle from the particle motion. This angle is still given by equation (1.26) [6], as is illustrated in the figure.

In practice, any left-handed medium must be highly dispersive, the left-handed behavior being restricted to some frequency range. Because the particle radiates at all frequencies, the Cerenkov radiation spectra must show wavefronts moving in both forward and backward directions [27].

1.6.3 Negative Goos–Hänchen Shift

When a plane wave is incident from a medium of refractive index $n = n_1$ onto the plane interface of another medium with $n = n_2$, where $|n_2| < |n_1|$, there is a critical angle $\sin \theta_c = |n_2/n_1|$, beyond which total reflection onto medium 1 occurs. However, fields penetrate into medium 2 by a small distance, forming a nonuniform plane wave that is evanescent in the direction normal to the interface and propagative along the interface. Power associated with this plane wave flows parallel to the interface in the forward direction for ordinary media and in the backward direction for left-handed media. Thus, when a beam of finite extent is incident from medium 1 to medium 2, the reflected beam experiences a finite lateral shift Δ, as a consequence of the aforementioned energy flow in medium 2. This effect is illustrated in Figure 1.6. As energy flow is parallel to wavefront propagation, the Goos–Hänchen shift must be positive in ordinary media. However, if medium 2 is a left-handed medium, energy flow and wavefront propagation are antiparallel. Therefore, the Goos–Hänchen shift must be negative in such media, as is illustrated in Figure 1.6*b*.

The Goos–Hänchen shift Δ can be calculated by expanding the incident beam in plane waves, and studying the reflection of these waves at the interface. If the angular spectrum of the beam is not too wide, and the angle of incidence is sufficiently away from the critical and grazing angles, the Goos–Hänchen shift is given by [28]

$$\Delta = \frac{\partial \phi_r}{\partial k_{\parallel}}, \tag{1.27}$$

where ϕ_r is the phase of the reflection coefficient and k is the component of the wavevector parallel to the interface (for lossless left-handed media $|r| = 1$, and $\phi_r = -j \ln r$). The Goos–Hänchen effect in left-handed media has been analyzed in detail in [29–32]. In [33], giant Goos–Hänchen shifts due to the excitation of surface waves have been reported for stratified media including left-handed layers. In all these calculations, the sign of the Goos–Hänchen shift agrees with the predictions of Figure 1.6.

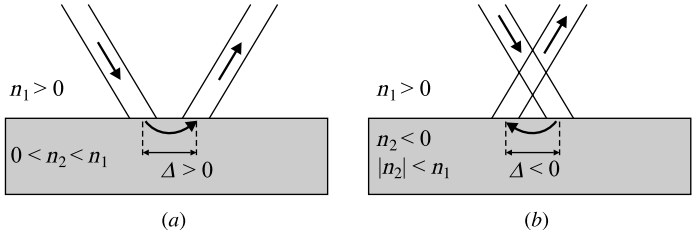

FIGURE 1.6 Illustration of the Goos–Hänchen effect in (*a*) ordinary media and (*b*) left-handed media.

1.7 WAVES AT INTERFACES

So far, our analysis has been developed in the frame of the geometrical optics approximation, although with some general considerations regarding electromagnetic wave analysis. In this section we will describe in more detail the electromagnetic interactions at the interface between a left-handed medium and an ordinary medium. We will consider s-polarized waves, so that electromagnetic fields are transverse electric (or TE) along the normal to the interface (these waves are also called *longitudinal section electric*, or LSE, waves). The analysis of p-polarized (*transverse magnetic*, TM, or *longitudinal section magnetic*, LSM) waves is quite similar, and the main results can be deduced from the results for s-polarized waves by means of a duality transformation [14] (see Problem 1.7). In this and the following section we will consider transparent lossless media. Thus, unless explicitly specified, losses will be neglected, so that ε and μ will be real quantities. This approximation, although nonphysical, is useful when losses can be considered small and propagative effects dominate.

1.7.1 Transmission and Reflection Coefficients

Transmission and reflection coefficients at the interface between an ordinary medium and a left-handed medium can be found using standard electromagnetic techniques. In this section we will follow the transverse transmission matrix [34] method. For this purpose, plane waves at both sides of a plane interface will be decomposed into propagative positive (+) and negative (−) waves, with a common wavevector component parallel to the interface (the k_z component in Fig. 1.7). For the plane

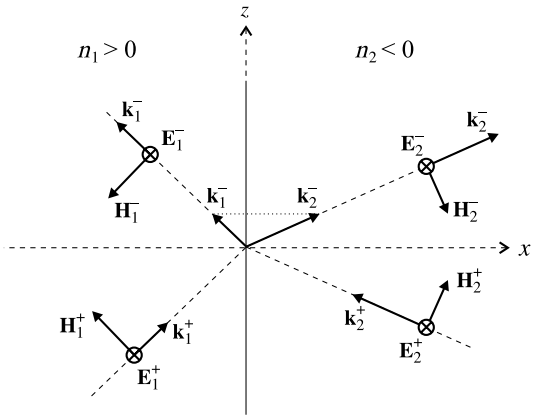

FIGURE 1.7 Definition of positive and negative waves for the determination of the transverse transmission matrix at the interface between an ordinary medium and a left-handed medium. Note that backward propagation in the left-handed medium has been taken into account in the definition of positive and negative waves.

interface shown in Figure 1.7, and for the considered s-polarized waves,

$$E_i \equiv E_{y,i} = E_i^+ + E_i^-, \tag{1.28}$$

where subindex $i = 1$ ($i = 2$) stands for the fields at the left-(right-)hand side of the interface (at $x = 0$). Positive waves are defined as those waves carrying energy along the positive axis perpendicular to the interface. Thus, if the interface is perpendicular to the x-axis, as in Figure 1.7, the field dependence of positive and negative waves can be summarized as

$$E_i^{\pm} \equiv E_{y,i}^{\pm} \propto \exp(\mp jk_{x,i}x - jk_z z + j\omega t), \tag{1.29}$$

where k_z is the common wavevector component parallel to the interface. According to backward propagation, in the left-handed half space, $k_{x,2} = \sqrt{\omega^2\varepsilon_2\mu_2 - k_z^2}$ must be chosen with $\mathrm{Re}(k_{x,2}) < 0$. For ordinary media $k_{x,1}$ must be chosen with $\mathrm{Re}(k_{x,1}) > 0$, as usual.

A key magnitude in our analysis is the wave impedance of each medium, Z_i, which is defined as the ratio between the transverse (to x) components of the electric and magnetic fields for positive waves propagating in such media. For the considered TE waves, a straightforward calculation leads to the result [1,34]

$$Z_i \equiv \frac{E_i^+}{H_{z,i}^+} = \frac{\omega\mu_i}{k_{x,i}}, \tag{1.30}$$

where $E_i^+ \equiv E_{y,i}^+$ is the electric field component of the positive wave. As both μ_2 and $k_{x,2}$ are negative in the left-handed medium, the impedance (1.30) is positive, as is required for passive media.

After expanding the transverse electric and magnetic fields at the left ($i = 1$) and the right ($i = 2$) sides of the interface into positive and negative waves ($E_i = E_i^+ + E_i^-$ and $H_{z,i} = H_{z,i}^+ + H_{z,i}^- = (E_i^+ - E_i^-)/Z_i$), and after imposing the continuity of the these field components at the interface, the transverse transmission matrix is determined as

$$\begin{pmatrix} E_1^+ \\ E_1^- \end{pmatrix} \equiv \bar{\bar{T}} \cdot \begin{pmatrix} E_2^+ \\ E_2^- \end{pmatrix} = \frac{1}{2Z_2}\begin{pmatrix} Z_2 + Z_1 & Z_2 - Z_1 \\ Z_2 - Z_1 & Z_2 + Z_1 \end{pmatrix} \cdot \begin{pmatrix} E_2^+ \\ E_2^- \end{pmatrix}. \tag{1.31}$$

From this result, the transmission, t, and reflection, r, coefficients are readily obtained by taking $E_1^+ = 1$, $E_1^- = r$, $E_2^+ = t$, $E_2^- = 0$; that is,

$$\begin{pmatrix} 1 \\ r \end{pmatrix} = \frac{1}{2Z_2}\begin{pmatrix} Z_2 + Z_1 & Z_2 - Z_1 \\ Z_2 - Z_1 & Z_2 + Z_1 \end{pmatrix} \cdot \begin{pmatrix} t \\ 0 \end{pmatrix}, \tag{1.32}$$

or

$$t = \frac{2Z_2}{Z_2 + Z_1} \qquad \text{and} \qquad r = \frac{Z_2 - Z_1}{Z_2 + Z_1}. \tag{1.33}$$

For the particular case of $Z_2 = Z_1$, from equations (1.33) it follows that $t = 1$ and $r = 0$. That is, the left-handed medium is perfectly matched with the ordinary medium. From equations (1.30) it follows that this is the case for any angle of incidence if $\varepsilon_2/\varepsilon_1 \to -1$ and $\mu_2/\mu_1 \to -1$.

Equations (1.33) are also valid when losses in the left-handed half space are taken into account. If, according to backward-wave propagation, we choose $\mathrm{Re}(k_{x,2}) < 0$ in equation (1.29), from equation (1.12) it follows that $\mathrm{Im}(k_{x,2}) < 0$. Therefore, positive waves carry energy and attenuate along the positive x-axis, as is required from energy conservation. Substitution of these values of $k_{x,2}$ in equations (1.30) and (1.33) gives the correct values for the transmission and reflection coefficients. Equations (1.33) are also valid for the total reflection case (i.e., when $k_z^2 > \omega^2\varepsilon_2\mu_2$), provided $k_{x,2}$ is chosen as $k_{x,2} = -j\alpha$, $\alpha = +\sqrt{k_z^2 - \omega^2\varepsilon_2\mu_2}$. In this case, Z_2 (1.30) is imaginary, and t and r become complex, with $|r| = 1$, as is required from energy conservation.

1.7.2 Surface Waves

Surface waves along the interface between two different media must decay at both sides of the interface. Therefore, imaginary values of $k_{x,i}$ should be considered. From the definitions of the previous section, it follows that

$$k_{x,i} = -j\alpha_i \qquad \text{and} \qquad \alpha_i = +\sqrt{k_z^2 - \omega^2\mu_i\varepsilon_i}, \tag{1.34}$$

in both ordinary and left-handed media. Therefore, positive waves in equation (1.29) will decay along the positive x-axis in both media. On the other hand, in order to obtain imaginary values of $k_{x,i}$, it must be that

$$k_z^2 > k_1^2, k_2^2, \tag{1.35}$$

where k_1 and k_2 are the wavevectors in the unbounded ordinary and left-handed media, respectively ($k_i^2 = \omega^2\varepsilon_i\mu_i$). With these definitions, surface waves correspond to solutions of the following implicit equation (see also equation (1.31):

$$\begin{pmatrix} 0 \\ E_1^- \end{pmatrix} = \frac{1}{2Z_2} \begin{pmatrix} Z_2 + Z_1 & Z_2 - Z_1 \\ Z_2 - Z_1 & Z_2 + Z_1 \end{pmatrix} \cdot \begin{pmatrix} E_2^+ \\ 0 \end{pmatrix}. \tag{1.36}$$

This equation has nontrivial solutions if $Z_2 + Z_1 = 0$. According to equations (1.30) and (1.34), Z_1 and Z_2 are both imaginary and have opposite signs in ordinary and left-handed media. Therefore, solutions to equation (1.36) can exist at the interface between these media, provided that expression (1.35) is satisfied. The general condition for the existence of such solutions is

$$k_z^2 = \frac{\mu_2^2 k_1^2 - \mu_1^2 k_2^2}{\mu_2^2 - \mu_1^2} > k_1^2,\ k_2^2, \tag{1.37}$$

which is also the dispersion relation for s-polarized (or TE, or LSE) surface waves. As both ε_2 and μ_2 strongly depend on frequency (see Section 1.3), the frequency dependence of $k_z(\omega)$ will depend on the specific characteristics of the left-handed medium. Dispersion curves for surface waves at the interface between free space and left-handed media have been investigated in [35,36] for some realistic frequency dependences of ε_2 and μ_2. It may be worth mentioning that similar surface waves (sometimes called surface plasmons) are guided along the interface between ordinary media and media with negative ε (see Problem 1.3). Surface waves can also be guided along the interfaces between ordinary and negative μ media, and at the interface between a medium with negative ε and other with negative μ [38].

Let us now consider again the limit $\varepsilon_2/\varepsilon_1 \to -1$ and $\mu_2/\mu_1 \to -1$. In this limit, the above dispersion relation becomes degenerate, being satisfied for any value of $k_z > k_1 = |k_2|$. Thus, in this limit, the bandwidth is zero and the density of states becomes infinite. This behavior is quite similar to that of surface plasmons at the surface of an ideal plasma in the quasistatic limit (see Problems 1.2 and 1.3). However, unlike for surface plasmons, the degeneracy of the considered surface waves is complete, not being restricted to the quasistatic limit (i.e., to $k_z \gg k_1 = |k_2|$).

Finally, due to the particular form of the transverse transmission matrix in equations (1.31) and (1.36), mathematical solutions corresponding to nonphysical surface waves growing to infinity at both sides of the interface show the same dispersion relation (1.37) as the aforementioned physical surface waves. Such solutions, although nonphysical for an isolated interface, will play an important role in the perfect lens configuration, as will be shown in the following.

1.8 WAVES THROUGH LEFT-HANDED SLABS

In this section, transmission and guidance of electromagnetic waves through left-handed slabs will be analyzed. The method of analysis will be a straightforward extension of the transverse transmission matrix technique of the previous section. The same method can be applied to the analysis of transmission and guidance of waves through multilayered structures.

1.8.1 Transmission and Reflection Coefficients

The transmission matrix for a left-handed slab of width d is obtained by simply cascading the transmission matrices for each interface (1.31) and for the left-handed medium in between,

$$\begin{pmatrix} E_1^+ \\ E_1^- \end{pmatrix} = \frac{1}{4Z_2Z_3} \begin{pmatrix} Z_2+Z_1 & Z_2-Z_1 \\ Z_2-Z_1 & Z_2+Z_1 \end{pmatrix} \cdot \begin{pmatrix} e^{jk_{x,2}d} & 0 \\ 0 & e^{-jk_{x,2}d} \end{pmatrix} \cdot \begin{pmatrix} Z_3+Z_2 & Z_3-Z_2 \\ Z_3-Z_2 & Z_3+Z_2 \end{pmatrix} \cdot \begin{pmatrix} E_3^+ \\ E_3^- \end{pmatrix}, \tag{1.38}$$

where, using the same notation as in equation (1.31), we have considered s-polarized waves. In equation (1.38) $k_{x,2} = -\sqrt{\omega^2\mu_2\varepsilon_2 - k_z^2} < 0$ is the x-component of the propagation constant for positive waves inside the slab, and subscripts 1, 2, and 3 stand for the left-handed medium (2) and for the media at the left- and the right-hand sides of the slab (1 and 3). Z_i are the wave impedances (1.30), and electric fields are evaluated just on the left ($E_1^{\pm}$) and on the right ($E_3^{\pm}$) interfaces of the slab. All waves inside and outside the slab have a common propagation vector, k_z, parallel to the slab interface, which determines the angle of incidence $\sin\theta_i = k_z/k_1$.

In the following, media 1 and 3 will be considered identical, so that $Z_3 = Z_1$. In this case, the transmission and reflection coefficients, t and r, are obtained from equation (1.38) by taking $E_1^+ = 1$, $E_1^- = r$, $E_3^+ = t$, $E_3^- = 0$. After a straightforward calculation, the following expressions arise:

$$t = \frac{2Z_1Z_2}{j(Z_1^2+Z_2^2)\sin(k_{x,2}d) + 2Z_1Z_2\cos(k_{x,2}d)} \tag{1.39}$$

and

$$r = \frac{Z_2^2 - Z_1^2}{Z_2^2 + Z_1^2 - 2jZ_1Z_2\cot(k_{x,2}d)}. \tag{1.40}$$

Note that $k_{x,2} < 0$, so the phase advance through the slab is positive for small values of $k_{x,2}d$, which corresponds to the propagation of a backward wave inside the slab.

1.8.2 Guided Waves

Waves guided along the slab correspond to the poles of the reflection coefficient (1.40) that may appear for imaginary values of $k_{x,1}$. In such cases, according to our previous definitions, $k_{x,1} = -j\alpha_1$, with $\alpha_1 = \sqrt{k_z^2 - \omega^2\varepsilon_1\mu_1} > 0$. Therefore,

surface waves correspond to solutions of the implicit equation

$$Z_2^2 + Z_1^2 - 2jZ_1Z_2\cot(k_{x,2}d) = 0, \qquad \text{with } Z_1 = j\frac{\omega\mu_1}{\alpha_1}, \tag{1.41}$$

with the additional condition $k_z > k_1$, so that electromagnetic energy decays at both sides of the slab. Two cases may arise in equation (1.41), depending on whether $k_{x,2}$ is real or imaginary. If $k_z < k_2 = \omega\sqrt{\varepsilon_2\mu_2}$, $k_{x,2}$ is real and fields inside the slab have a trigonometric dependence, so that they are *volume waves*. In that case equation (1.41) reduces to

$$\frac{\mu_2\alpha_1}{\mu_1 k_{x,2}} - \frac{\mu_1 k_{x,2}}{\mu_2\alpha_1} + 2\cot(k_{x,2}d) = 0, \tag{1.42}$$

which, taking into account the trigonometric relation $2\cot(2x) = \cot x - \tan x$, can be written as

$$\left(\frac{\mu_2\alpha_1}{\mu_1 k_{x,2}}\tan(k_{x,2}d/2) + 1\right)\left(\frac{\mu_1 k_{x,2}}{\mu_2\alpha_1}\tan(k_{x,2}d/2) - 1\right) = 0, \tag{1.43}$$

which is the implicit dispersion relation for guided volume waves. In equation (1.43) the two branches, corresponding to symmetric and antisymmetric modes, are explicitly shown. As can be seen from the above dispersion relations, volume waves in the left-handed slabs do not substantially differ from guided volume waves in ordinary dielectric slabs [34]; waves inside the slab can be seen as the composition of two propagating TEM waves, which suffer total reflection at the slab interfaces. Therefore energy flow is backward inside the left-handed slab and forward outside the slab, the whole wave being forward or backward depending on the structural parameters of the waveguide.

If $k_z > k_2 = \omega\sqrt{\varepsilon_2\mu_2}$, electromagnetic fields show an exponential decay inside the slab, and the guided waves become *surface waves*. They correspond to the coupling between the surface waves generated at each slab interface (see Section 1.7.2). Therefore, when $d \to \infty$, these waves should converge to the surface waves found in Section 1.7.2. For these surface waves, both Z_1 and Z_2 are imaginary and $\cot(k_{x,2}d)$ becomes a hyperbolic function. Thus, equation (1.41) reduces to

$$\frac{\mu_2\alpha_1}{\mu_1\alpha_2} + \frac{\mu_1\alpha_2}{\mu_2\alpha_1} + 2\coth(\alpha_2 d) = 0, \tag{1.44}$$

which, taking into account the relation $2\coth(2x) = \coth x + \tanh x$, can be written as

$$\left(\frac{\mu_2\alpha_1}{\mu_1\alpha_2}\tanh(\alpha_2 d/2) + 1\right)\left(\frac{\mu_1\alpha_2}{\mu_2\alpha_1}\tanh(\alpha_2 d/2) + 1\right) = 0, \tag{1.45}$$

where the two branches, corresponding to symmetric and antisymmetric modes, can be appreciated. The specific dependence of k_z on frequency will depend on the specific dependence of ε and μ on ω. Surface and volume guided waves in left-handed slabs, also including metallic ground shields, have been analyzed in [37–43]. Finally, it would be worth mentioning that resonant modes in other geometries distinct from planar ones, such as spherical or cylindrical, have been also studied (see, for instance, [44–47], and references therein).

1.8.3 Backward Leaky and Complex Waves

As in any open guiding system, most of the electromagnetic modes guided by a left-handed slab leak power to the surrounding space [13,34]. These waves correspond to the poles of the reflection coefficient (1.40) that may appear for complex values of $k_{x,1}$.

Leaky modes in a left-handed slab have been analyzed in [48]. In the following we will consider, without loss of generality, a leaky wave with field dependence $\exp(-jk_z z + j\omega t)$, and $\mathrm{Re}(k_z) > 0$. The wavenumber of such a leaky mode should satisfy $\mathrm{Re}(k_z) < k_1 \equiv \omega\sqrt{\varepsilon_1\mu_1}$, so that power leaks at an angle $\cos\theta = \mathrm{Re}(k_z)/k_1$ from the slab (Fig. 1.8). Inside the left-handed slab, power flow is backward, but in the surrounding medium, outside the slab, power flows in the forward direction. Therefore, for the analyzed leaky mode, power always leaks *backward* with regard to the main stream of guided power, inside the slab. For this reason, such leaky modes have been called *backward leaky modes* [48].

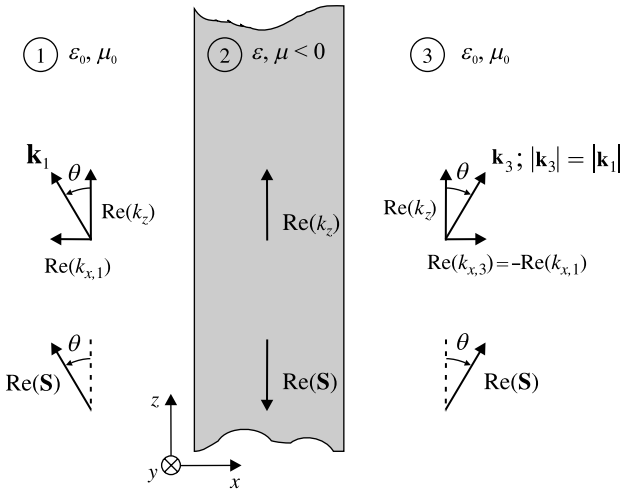

FIGURE 1.8 Illustration of the wavevectors and power flows in a backward leaky mode guided by a left-handed slab. $\mathrm{Re}(k_z)$ is the mode phase vector, and $\mathrm{Re}(\mathbf{S})$ shows the power flux inside and outside the slab. The angle of leakage is determined by $\cos\theta = \mathrm{Re}(k_z)/k_1$.

Physical leaky modes can be excited by sources at the onset of a semi-infinite guiding system. In such a configuration, power is guided along the waveguide, from the source to its end. Considering Figure 1.8, this means that the source must be located at the top of the figure. Therefore, it must be that $\mathrm{Im}(k_z) > 0$, so that the leaky wave attenuates towards the lower end of the slab. On both sides of the slab the field dependence must be of the kind $\exp(\mp jk_x x - k_z z + j\omega t)$. On the other hand, boundary conditions impose that $k_z^2 + k_x^2 = k_1^2$, so that, for small attenuating constants,

$$k_1^2 \simeq \{\mathrm{Re}(k_z)\}^2 + \{\mathrm{Re}(k_x)\}^2 \tag{1.46}$$

$$0 = \mathrm{Re}(k_z)\mathrm{Im}(k_z) + \mathrm{Re}(k_x)\mathrm{Im}(k_x). \tag{1.47}$$

The first equation defines the leakage angle mentioned at the beginning of this section. The second determines the sign of $\mathrm{Im}(k_x)$ as follows: at the left-hand side of the slab, power must flow to the left, so that $\mathrm{Re}(k_z) > 0$ and $\mathrm{Re}(k_x) < 0$. Moreover, $\mathrm{Im}(k_z) > 0$, as has already been mentioned. Therefore, it must be that $\mathrm{Im}(k_x) > 0$, so that backward leaky waves are attenuated in the transverse direction. This result is somewhat unexpected, as leaky modes in ordinary guiding systems are usually unbounded modes, whose amplitude grows to infinity in the transverse direction [34,49]. This unusual behavior of leaky modes in left-handed slabs is a direct consequence of the reported backward leakage of power [48], and recalls the behavior of the complex modes that may appear in some very inhomogeneous wave-guiding systems [13]. Backward leakage of power in a circuit analogous to an open left-handed waveguide has been experimentally reported in [50].

1.9 SLABS WITH $\varepsilon/\varepsilon_0 \to -1$ AND $\mu/\mu_0 \to -1$

As has already been mentioned, many striking properties of left-handed media arise in the limit when ε and μ become equal in magnitude, but opposite in sign, as in those of the surrounding medium. In this section we will analyze these properties in detail. For simplicity, the surrounding medium is considered free space.

1.9.1 Phase Compensation and Amplification of Evanescent Modes

If $\varepsilon/\varepsilon_0 \to -1$ and $\mu/\mu_0 \to -1$, the left-handed wave impedances (1.30) of the left-handed medium become identical to that of free space for any propagative wave, and for any angle of incidence. Therefore, for any angle of incidence, the transmission matrix at each slab interface (1.31) reduces to unity. Thus, the slab is perfectly matched to free space. Even more interesting, because wave propagation is backward inside the left-handed slab, the phase advance inside the slab is positive, and can be exactly compensated by the phase advance outside the slab (which must be negative). A straightforward calculation shows that this compensation actually happens—for

any angle of incidence—when the distance between the input and output planes is $2d$, where d is the slab width. In fact, this last property is a direct consequence of the zero optical length between the input and output planes already mentioned in Section 1.5

Let us now consider the incidence of evanescent waves on the slab. In this case, after substitution in equations (1.30), (1.39), and (1.40) (with $k_{x,1} = k_{x,2} = -j\alpha$; $\alpha = +\sqrt{k_z^2 - \varepsilon_0\mu_0}$), it is readily shown that

$$t = e^{\alpha d} \qquad \text{and} \qquad r = 0. \tag{1.48}$$

Thus, evanescent plane waves are *amplified* inside the left-handed slab by a factor that is just the attenuation constant at the input. Because evanescent modes do not carry energy, this amplification, although striking, is not forbidden by energy conservation. Interestingly, when the input and output planes are separated by a distance $2d$, the amplitude of any incident evanescent wave is recovered at the output. Thus, for this specific location of the input and output planes, both propagating and evanescent waves are recovered without change at the output.

Phase compensation and amplification of evanescent modes is not a unique property of left-handed slabs. After attention was first drawn to this effect by Pendry [26], it was also shown in a pair of consecutive slabs with only negative ε and μ [51,52] and, for some specific polarizations and planes of incidence, in some anisotropic slabs with negative parameters [53]. It has also been shown in a pair of coupled resonant surfaces [54]. Some of these results have been summarized in a *generalized perfect lens theorem* [55].

1.9.2 Perfect Tunneling

As is well known, when a wave is incident from a medium of refractive index $n = n_1$ onto the plane interface of another medium of $n = n_2$, where $|n_2| < |n_1|$, there is a critical angle $\theta_c = \sin^{-1}|n_2/n_1|$ beyond which total reflection onto medium 1 occurs. However, if medium 2 is substituted by a slab of finite thickness, and the slab is not too thick, some amount of energy can tunnel through medium 2 onto the medium behind the slab. For ordinary media, the power tunneled through the slab is always smaller than the incident power, so there is also some reflected power. This tunneling of power is due to the coupling of evanescent waves generated at both sides of the slab. Thus, because a left-handed slab can restore the amplitude of evanescent waves (as was shown in the previous section), it can be guessed that tunneling through left-handed slabs can be very significant. In fact, as will be shown in this section, under some circumstances such tunneling of power can be so high that all the incident power will flow through the slab. This "perfect tunneling" effect will be analyzed in this section.

Instead of analyzing incidence in free space, a different but fully equivalent system will be analyzed. This system is shown in Figure 1.9, and consists of a rectangular waveguide that includes a section filled with a left-handed medium with $\varepsilon/\varepsilon_0 \to -1$ and

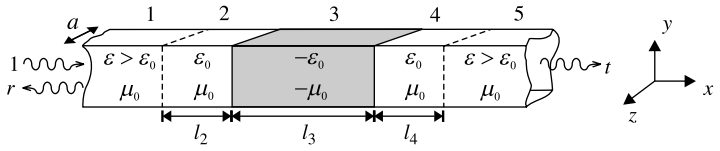

FIGURE 1.9 Illustration of a device designed to study perfect tunneling and amplification of evanescent waves in a waveguide. The device consists of five consecutive waveguides with the same cross-section. Input and output waveguides (1 and 5) are above cutoff. Waveguides 2 to 4 are below cutoff. Waveguides 2 and 4 are empty. Waveguide 3 is filled with an isotropic left-handed medium with $\varepsilon = -\varepsilon_0$, $\mu = -\mu_0$, and $l_3 = l_2 + l_4$.

$\mu/\mu_0 \rightarrow -1$. As is well known [1,34], the fundamental mode in a rectangular waveguide is the $TE_{1,0}$ mode, which corresponds to the composition of two propagating s-polarized plane waves ($\mathbf{E} = E_y\,\hat{\mathbf{y}}$), which are reflected by the lateral sidewalls of the waveguide, giving rise to a stationary wave in the transverse direction and a propagating wave along the waveguide axis: $E_y \propto \sin(\pi z/a)\exp(-jk_x x + j\omega t)$. This mode is propagative/evanescent if the waveguide width is larger/smaller than a half-wavelength ($a \gtrless \pi/k$, where $k = \omega|\sqrt{\mu\varepsilon}|$). Therefore, evanescent plane waves are generated in sections 2 to 4 of Figure 1.9 if $a < \pi/k_0$, where $k_0 = \omega\sqrt{\mu_0\varepsilon_0}$. In order to excite this evanescent mode, we can simply place at the input a waveguide filled by a high-permittivity dielectric, supporting a propagative $TE_{1,0}$ mode incident on section 2 (if the cross-sections of both waveguides are identical, no other modes will be generated at the interface [34]). It can be easily realized that such a system is equivalent to the incidence of two identical s-polarized waves coming from a semi-infinite medium (medium 1) onto a slab formed by media 2 to 4, and with a semi-infinite medium (medium 5) at the end of the system. The angle of incidence is $\theta = \sin^{-1}\{\pi/(ka)\}$, where $k^2 = \omega^2\varepsilon\mu_0$, and incidence by an angle higher than the critical angle corresponds to the excitation of evanescent modes at waveguide sections 2 to 4 of Figure 1.9. Thus, a system such as that shown in this figure is fully equivalent, from an analysis standpoint, to a composite slab made of media 2 to 4, sandwiched between two semi-infinite media (1 and 5). However, the system of Figure 1.9 is easier to implement for an experimental verification of tunneling effects.

Let us now analyze the behavior of the device. When a propagative $TE_{1,0}$ mode is incident from waveguide 1, evanescent $TE_{1,0}$ modes are generated in waveguides 2 to 4 and, eventually, some power may tunnel to waveguide 5. Following our previous analysis, transmission and reflection coefficients can be obtained from the implicit equation

$$\begin{pmatrix} 1 \\ r \end{pmatrix} = \frac{1}{2Z_2}\begin{pmatrix} Z_2+Z_1 & Z_2-Z_1 \\ Z_2-Z_1 & Z_2+Z_1 \end{pmatrix}\cdot\begin{pmatrix} e^{\alpha_2 l_2} & 0 \\ 0 & e^{-\alpha_2 l_2} \end{pmatrix}$$
$$\cdot\frac{1}{2Z_3}\begin{pmatrix} Z_3+Z_2 & Z_3-Z_2 \\ Z_3-Z_2 & Z_3+Z_2 \end{pmatrix}\cdot\begin{pmatrix} e^{\alpha_3 l_3}, & 0 \\ 0, & e^{-\alpha_3 l_3} \end{pmatrix}$$

$$\cdot \frac{1}{2Z_4}\begin{pmatrix} Z_2+Z_3 & Z_2-Z_3 \\ Z_2-Z_3 & Z_2+Z_3 \end{pmatrix} \cdot \begin{pmatrix} e^{\alpha_2 l_4} & 0 \\ 0 & e^{-\alpha_2 l_4} \end{pmatrix}$$
$$\cdot \frac{1}{2Z_1}\begin{pmatrix} Z_1+Z_2 & Z_1-Z_2 \\ Z_1-Z_2 & Z_1+Z_2 \end{pmatrix} \cdot \begin{pmatrix} t \\ 0 \end{pmatrix}, \tag{1.49}$$

where α_i are the attenuation constants of the $TE_{1,0}$ mode in waveguides 2, 3, and 4 ($\alpha_i = +\sqrt{(\pi/a)^2 - \omega^2\mu_i\varepsilon_i}$), and Z_i are the wave impedances (1.30) for each mode, with $k_{x,i} = -j\alpha_i$,

$$Z_i = j\frac{\omega\mu_i}{\alpha_i}; \qquad i = 2, 3, 4. \tag{1.50}$$

In the limit $\varepsilon/\varepsilon_0 \to -1$ and $\mu/\mu_0 \to -1$, $Z_3 = -Z_2$, and we obtain

$$t = 1 \text{ and } r = 0, \quad \text{for } l_2 + l_4 = l_3. \tag{1.51}$$

That is, total transmission is obtained for the appropriate waveguide lengths. This total transmission is not a Fabry–Perot resonance, because all waves between the input and the output are evanescent. It is a perfect tunneling of power between input and output [56].

Interestingly, the condition for perfect tunneling coincides with the condition for focusing (1.22) when $n = -1$, and with the condition for amplitude and phase restoration (see Sections 1.4 and 1.9.1). In fact, if $l_2 + l_4 \neq l_3$, the amount of power tunneled through the device decreases. This effect is illustrated in Figure 1.10, where the

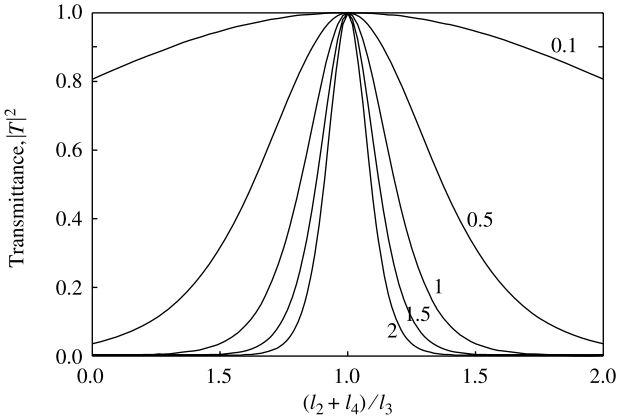

FIGURE 1.10 Transmitted power through the device of Figure 1.9 versus the ratio $(l_2 + l_4)/l_3$ for several values of l_3/λ_0 (values given close to the lines). The waveguide width is $a = 0.8\,\lambda_0/2$. The dielectric constant of sections 1 and 5 is $\varepsilon = 2\varepsilon_0$. (*Source*: Reprinted with permission from [56]; copyright 2005 by the American Physical Society.)

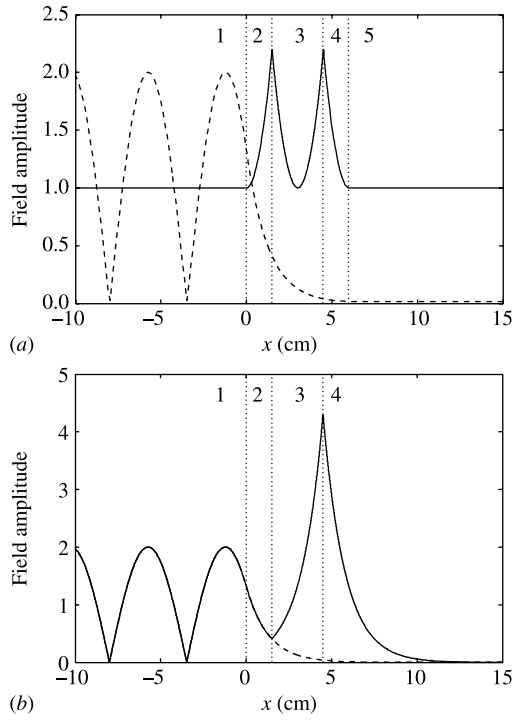

FIGURE 1.11 Field amplitude distribution inside the structure of Figure 1.9. (*a*) Perfect tunneling when $l_3 = l_2 + l_4$. (*b*) Field amplitude when the last transition is eliminated ($l_4 \to \infty$). Dashed lines show the amplitude when waveguide 3 is empty. Geometrical dimensions are $a = 24\,\text{mm}$, $l_2 = l_4 = 15\,\text{mm}$, $l_3 = 30\,\text{mm}$, and the operating frequency is 5 GHz. The dielectric constant of sections 1 and 5 is $\varepsilon = 2\varepsilon_0$. (*Source*: Reprinted with permission from [56]; copyright 2005 by the American Physical Society.)

fraction of power tunneled through the device is shown as a function of $(l_2 + l_4)/l_3$. The sensitivity of the device to the normalized length of the left-handed slab l_3/λ_0 (λ_0 is the free-space wavelength at the frequency of operation) can also be observed. As can be expected, this sensitivity is higher for larger slabs.

In order to clarify the relation between perfect tunneling and amplification of evanescent waves, it is illustrative to analyze field amplitudes along the device of Figure 1.9 for the perfect tunneling configuration, and when the output waveguide is eliminated ($l_4 \to \infty$).[2] Both amplitudes are shown in Figure 1.11. Amplification of the evanescent wave inside the left-handed medium can be clearly appreciated in Figure 1.11*b*. The restoration of the mode amplitude at a distance $2l_3$ from the input can also be appreciated in this figure. However, the pattern for the wave amplitude is quite different in the perfect tunneling configuration (Fig. 1.11*a*). The reason

[2]Such amplitudes can be obtained from the amplitudes at the input by cascading the appropriate transmission matrices between the input and the plane of interest.

for this is that single evanescent modes do not carry power, and perfect tunneling implies a maximum of power transmission. To obtain this transmission peak, the composition of two symmetrical evanescent modes decaying at opposite directions is necessary. This leads to the amplitude pattern shown in Figure 1.11*a*.

Perfect tunneling of power through waveguides filled by metamaterials with negative parameters was proposed and demonstrated in [56], where an experimental verification of this effect was also provided. Photon tunneling through a left-handed slab in free space was analyzed in [57].

1.9.3 The Perfect Lens

The perfect lens is one of the most fascinating devices that can be designed by using the striking optical properties of left-handed materials. This configuration was first proposed by Pendry in his seminal paper of 2000 [26]. In this paper Pendry showed how the amplitude of evanescent waves can be restored by a left-handed slab, and how using this property, a perfect lens overcoming the diffraction limit for the resolution of conventional lenses can be designed.

Before showing how the properties of left-handed slabs can be used to improve lens resolution, the limitations imposed by Fourier optics to the resolution of a lens will be described in detail. Following [26], we will consider an infinitesimal dipole of frequency ω in front of a lens. The electric field produced by this dipole can be expanded in some two-dimensional Fourier integral of plane waves (spatial Fourier harmonics),

$$\mathbf{E}_{\mathrm{p}}(x, y, z) = \int_{-\infty}^{\infty} \mathrm{d}k_y \int_{-\infty}^{\infty} \mathrm{d}k_z \, \mathbf{E}(k_y, k_z) \, \exp(-jk_x x - jk_y y - jk_z z + j\omega t), \qquad (1.52)$$

where $k_x = \sqrt{\omega^2 \varepsilon_0 \mu_0 - k_y^2 - k_z^2}$. The response of any optical system to this excitation can be obtained by analyzing the scattering of each plane wave of (1.52), and then adding up for all the scattered waves. However, optical systems are usually only sensitive to propagating waves, that is, to waves with real values of k_x (the x-axis is assumed to be the axis of the system). Evanescent waves are usually strongly attenuated and do not reach the image. Therefore, even for the best manufactured lens, the resolution at the image is limited by the truncation of the expansion (1.52) to

$$\mathbf{E}_{\mathrm{p}}(x, y, z) \simeq \int\int_{-k_{\max}}^{k_{\max}} \mathrm{d}k_y \, \mathrm{d}k_z \, \mathbf{E}(k_y, k_z) \, \exp(-jk_x x - jk_y y - jk_z z + j\omega t), \qquad (1.53)$$

where $k_{\max} = k_0 = \omega\sqrt{\varepsilon_0 \mu_0}$. Equation (1.53) gives the *effective* source seen by the optical system. Therefore, from a well-known rule of Fourier analysis, it immediately follows that the aforementioned infinitesimal dipole is restored at the image with a resolution Δ not better than a wavelength ($\Delta \geq 2\pi/k_0 = \lambda_0$).

The above analysis is based on the assumption that any lens or optical system will lose all the information contained in the evanescent Fourier harmonics of the source

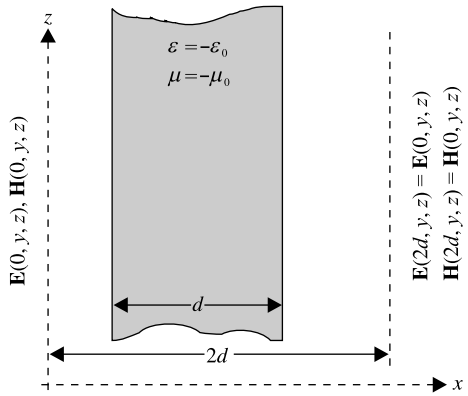

FIGURE 1.12 Illustration of the perfect lens proposed in [26]. The fields at $x = 0$ ($\mathbf{E}(0, y, z)$ and $\mathbf{H}(0, y, z)$) are exactly reproduced at $x = 2d$: $\mathbf{E}(0, y, z) = \mathbf{E}(2d, y, z)$ and $\mathbf{H}(0, y, z) = \mathbf{H}(2d, y, z)$, provided there are no sources between the planes $x = 0$ and $x = 2d$.

field expansion (1.52). However, we have already seen how a left-handed slab of width d, and $\varepsilon/\varepsilon_0 \to -1$, $\mu/\mu_0 \to -1$ can restore the amplitude and phase of any incident plane wave at a distance $2d$ from the input, both for propagative and evanescent waves. Therefore, it is the whole field at the source (1.52) that is restored at $x = 2d$, not the truncated expansion (1.53). That is, left-handed slabs in the limit $\varepsilon/\varepsilon_0 \to -1$ and $\mu/\mu_0 \to -1$ behave as perfect lenses, translating the whole field distribution on a plane at the left side of the slab to another plane at the right side of the slab, as is shown in Figure 1.12.

It is illustrative to analyze the role of surface waves in the restoration of the evanescent Fourier harmonics at the image plane. Figure 1.13 shows the amplitude pattern for one of these evanescent Fourier harmonics between $x = 0$ and $x = 2d$. The physical and nonphysical surface waves mentioned at the end of Section 1.7.2 can be easily recognized in the amplitude curves of Figure 1.13. Therefore, the restoration of an evanescent Fourier harmonic in the perfect lens is due to the excitation of a physical surface wave at the right interface of the slab. This physical surface wave couples with the evanescent fields generated at the source through the excitation of a nonphysical (see the end of Section 1.7.2) surface wave[3] at the left interface of the slab. It may be worth mentioning that this field pattern does not imply that an actual surface wave is generated at the slab. In fact, it can be easily realized that equation (1.45) has no solutions for $\varepsilon/\varepsilon_0 = \mu/\mu_0 = -1$ (except for the trivial case of $d \to \infty$). In fact, the generation of such slab surface waves would be undesirable, because it would imply a disproportionate contribution of the corresponding Fourier harmonic to the image.

[3]The denomination "nonphysical" indicates that these waves do not satisfy physical boundary conditions at infinity when they are considered in an unbounded system (they monotonically grow at both sides of the interface). However, the presence of additional boundary conditions, as in Figure 1.13, allows for its excitation.

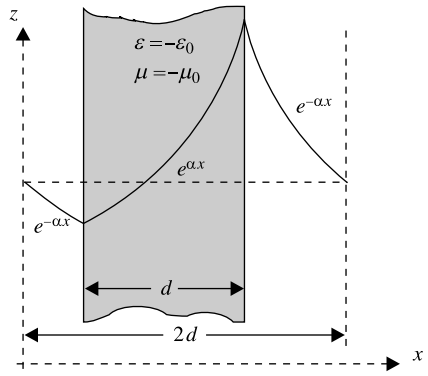

FIGURE 1.13 Amplitude pattern for an evanescent Fourier harmonic of the perfect lens shown in Figure 1.12. The amplitude follows the curves $\exp(\pm\alpha x)$, where $\alpha(k_y, k_z) = \sqrt{k_y^2 + k_z^2 - \omega^2\varepsilon_0\mu_0}$.

Some considerations should be made at this point. First of all, as has already been mentioned, restoration of evanescent Fourier harmonics at $x = 2d$ implies the amplification of such Fourier harmonics inside the slab (Fig. 1.13). As we approach the back interface of the slab, the density of energy stored by these evanescent waves grows by the exponential factor $\exp[2\alpha(d - \delta)]$, where δ is the distance to the interface. In the limit $|k_z|, |k_y| \to \infty$, we have $\alpha(k_y, k_z) = \sqrt{k_x^2 + k_y^2 - \omega^2\varepsilon_0\mu_0} \to \infty$, and the density of energy grows to infinity at the slab interface. Therefore, the perfect lens implies a nonphysical divergence of energy [58]. Although we will return to this point later (see Section 1.10) it should be mentioned here that this apparent paradox disappears if lossy slabs are considered [59–61]. An additional effect of losses is to limit the resolution of the perfect lens. Lossy left-handed slab lenses can still improve the value of $k_{\max}$ ($k_{\max} > \omega\sqrt{\varepsilon_0\mu_0}$) in equation (1.53), but leaving it finite (see Section 1.10 for a complete discussion on this point). Therefore, it will be more appropriate to speak about lossy left-handed superlenses, which approach Pendry's perfect lens when losses approach to zero.

Other considerations of interest arise from the comparison between the Veselago lens (see Fig. 1.3) and Pendry's perfect lens. For this purpose we will consider the image of a point source created by both lenses. A Veselago lens, with $n < 0$ but $\varepsilon/\varepsilon_0\,, \mu/\mu_0 \neq -1$, will be considered first. It is a nonconventional geometrical optics system, where electromagnetic energy coming from a point source is focused into a three-dimensional spot beyond the lens, of radius not smaller than a half wavelenght (this behavior is sketched in Fig. 1.14*a*). Therefore, superresolution is not present in the Veselago lens. Let us now consider Pendry's perfect lens. In this device, the fields at $x = 0$, where the source is placed, are exactly reproduced at $x = 2d$ (see Fig. 1.12). Therefore, from the uniqueness theorem [14], it immediately follows that the source fields in the x-interval $[0, \infty]$ are exactly reproduced beyond the lens in the x-interval $[2d, \infty]$. However, nothing ensures that the source

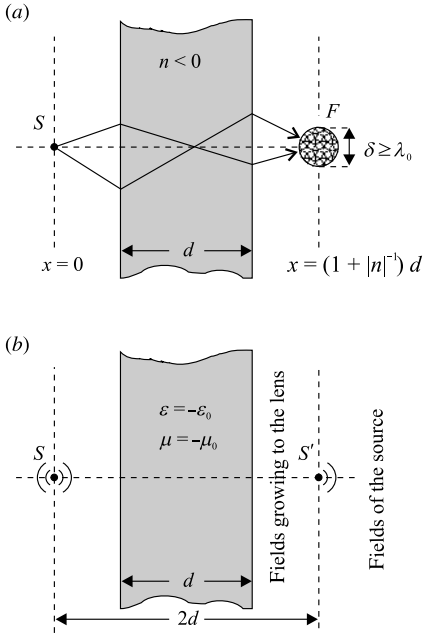

FIGURE 1.14 Illustration of the behavior of the Veselago (*a*) and Pendry (*b*) lenses. In the Veselago lens the energy coming from a point source, S, is focused onto a spot at the focus, F, at a distance $d + d/|n|$ from the source. The size of this spot is not smaller than a wavelength. In Pendry's perfect lens, a virtual image, S', of a point source, S, is created at a distance $2d$ from S. However, fields at $x < 2d$ grow exponentially towards the lens, so there is no focusing of energy at any point.

fields for $x < 0$ will be reproduced at $x < 2d$. In fact, this will be impossible, as the presence of the source implies a field divergence at $x = 0$ that is not present at $x = 2d$ [62]. Intuitively, it can be guessed from the amplitude pattern of Figure 1.13 that fields must grow from the image plane to the lens, regardless of behavior near the source (such behavior is sketched in Fig. 1.14*b*). In fact, this behavior has been confirmed by analysis [63] and experiment [64]. Therefore, Pendry's perfect lens does not focus the energy coming from a point source into any spot in three-dimensional space. Nevertheless, it still produces a two-dimensional spot on the image plane ($x = 2d$), of a size that can be much smaller than a square wavelength. Therefore, Pendry's perfect lens produces two-dimensional superresolution in the image plane, but not superfocusing of energy in three-dimensional space[4]. This characteristic of the perfect lens (and similar devices) imposes severe limitations to its applicability for subsurface heating or burning devices. It also imposes restrictions on its usefulness

[4]Such three-dimensional superfocusing will be contrary to the well-known uncertainty principle, as has already been noted in [65] and [66]. It should also be mentioned that any practical lens must be lossy, and that the behavior of lossy Pendry's superlenses approaches that of Veselago lenses when the ratio d/λ_0 increases (see Section 1.10).

in imaging devices, at least if the distance between the source and the lens is unknown. In fact, because the electromagnetic field intensity has a monotonic decay at the back side of the lens, the location of an unknown source can hardly be recovered from the analysis of the field distribution at the back side of the lens (see [63] for a complete discussion, with examples, of this point).

Experimental confirmation of subdiffraction imaging in Pendry's perfect lens has been reported in [64], and the effects of an input or output medium other than free space have been investigated in [67] (see Problem 1.13). Superresolution similar to that produced by a left-handed perfect lens, but in the quasistatic limit, can be obtained by using slabs with only negative ε (such as silver plates at optical frequencies) [26,68–71] (see Problem 1.14). It can be also obtained in magnetized ferrite slabs [72] and in pair-coupled magnetoinductive surfaces [73].

1.9.4 The Perfect Lens as a Tunneling/Matching Device

In the previous section, the field created by a source placed in front of a perfect lens was studied. In this section we will address the problem of image detection in such devices. A key point in the behavior of Pendry's perfect lens is that most of the information reaching the image plane is carried by evanescent electromagnetic waves (the aforementioned evanescent Fourier harmonics). As is well known, a single evanescent electromagnetic wave does not carry power (for this reason the amplification of evanescent Fourier harmonics inside the lens does not violate energy conservation). However, any measurement of the image should imply the transmission of some amount of power from the source to the detector. Power transmission by evanescent waves is known in physics as *tunneling*. Therefore, seen from the detector, a *perfect lens* is a kind of tunneling device. For a single electromagnetic mode, tunneling of power was analyzed in Section 1.9.2. For a summation of evanescent waves (the aforementioned evanescent Fourier harmonics), the basic mechanism should be essentially the same: Some *new* evanescent waves are generated at the output in addition to the evanescent Fourier harmonics generated by the source. It is the composition of all these waves that allows for power transmission. The aforementioned *new* evanescent waves generated at the output are not present *before* the detector is placed at the output. Therefore, the image detection process substantially affects the field distribution along the system formed by the source and the lens. These kind of devices, where fields depends on both the input and the output, have long been considered by electrical engineers. Some of these devices—those that maximize power flow—are usually called *matching* devices. Thus, from this standpoint, the perfect lens can also be considered a matching device [66,74].

In the following we will analyze the image detection process in detail. As usual, we will consider a system formed by the perfect lens, an input antenna (the source S), and an output antenna (the detector D). Two waveguides are connected to the input and output antennas (for simplicity both waveguides will be assumed identical, with characteristic impedance Z_0). The image is obtained by scanning the detector behind the lens, as a map of the transmission coefficient between the source and the detector. The whole system is illustrated in Figure 1.15. The computation of the transmission

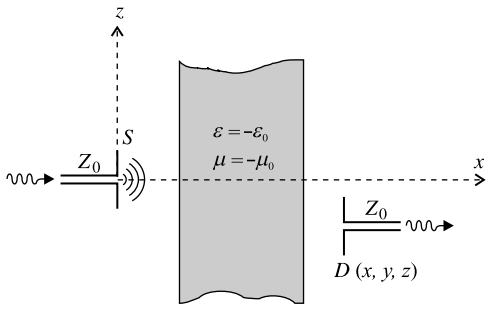

FIGURE 1.15 Experimental setup for the detection of images created by a left-handed perfect lens. The source S is placed at a fixed distance from the left-handed slab, and the detector D is scanned behind the slab. The transmission coefficient between S and D is measured.

coefficient is a standard problem of electromagnetic theory, which can be solved if the impedance matrix Z_{ij} of the system formed by the antennas and the lens is known. The resulting expression is [75]

$$t = \frac{2Z_{12}Z_0}{(Z_{11} + Z_0)(Z_{22} + Z_0) - Z_{12}^2}, \tag{1.54}$$

where Z_{ij} are the elements of the impedance matrix of the system formed by the two antennas and the left-handed slab, and Z_0 is the characteristic impedance of the input/output waveguides. If superresolution has to be detected, the size of the input and output antennas has to be smaller than the free-space wavelength, which would also make the real part of Z_{ij} (the radiation resistance) negligible with respect to its imaginary part [14]; in other words, $Z_{ij} \simeq jX_{ij}$, where X_{ij} is the reactance matrix of the system[5]. Moreover, because the perfect lens perfectly matches any source to free space, X_{11} and X_{22} can be approximated by the reactances of the input and output antennas in free space. The off-diagonal term, X_{12}, accounts for the mutual reactance between the antennas, which is strongly affected by the presence of the lens. Therefore,

$$t \approx \frac{2jX_{12}Z_0}{(jX_{11} + Z_0)(jX_{22} + Z_0) + X_{12}^2}. \tag{1.55}$$

If one of the self-reactances dominates over the remaining ones, the first term in the denominator of (1.55) dominates over the second, and

$$t \propto X_{12}. \tag{1.56}$$

[5]Throughout this section we will consider lossless antennas. Loading the antennas with a resistance has consequences that will not be analyzed here. See [63] for an analysis of this particular scenario.

That is, the transmission coefficient is simply proportional to the mutual reactance, X_{12}, which usually provides a good measure of the field in the absence of the output. This case may correspond to a small electric dipole antenna at the output (in such a case, $|X_{22}| \gg |X_{21}|, |X_{11}|$). It may also occur when the output antenna is a small magnetic loop (in such a case, usually, $|X_{11}| \gg |X_{21}|, |X_{11}|$, [63]). Therefore, if small electric or magnetic probes are used as detectors, the transmission coefficent through the device can give a correct measurement of the field created by the source at the back side of the lens. This result can be expected from the physics of the experiment; in both cases the field generated by the currents at the output antenna should be very small, and should not substantially affect either the current at the input antenna or the field distribution behind the lens. As was shown in [64], when such a small probe is used for field measurements at the back side of the lens, the maximum of transmission is obtained just at the back interface of the lens, in agreement with the behavior outlined in Figure 1.14.

However, if the self-reactances of the input and output antennas are the same ($X_{11} = X_{22} = X$), which may corresponds to a detector identical to the source, then

$$t \approx \frac{2jX_{12}Z_0}{X_{12}^2 - X^2 + Z_0^2 + 2jXZ_0} \,. \tag{1.57}$$

The values of t, as a function of X_{12} and X, are plotted in Figure 1.16. Except for very small values of X, the maximum is achieved for $X_{12} \approx X$, and in such a case it is also the case that $|t| \approx 1$. Because both antennas are identical and the lens reproduces the field of the source at the image plane, the condition $X_{12} \approx X$ is fulfilled when the detector is placed at the theoretical location of the image, at a distance $2d$ from the source. Therefore, if the source and the detector are identical, and the detector is

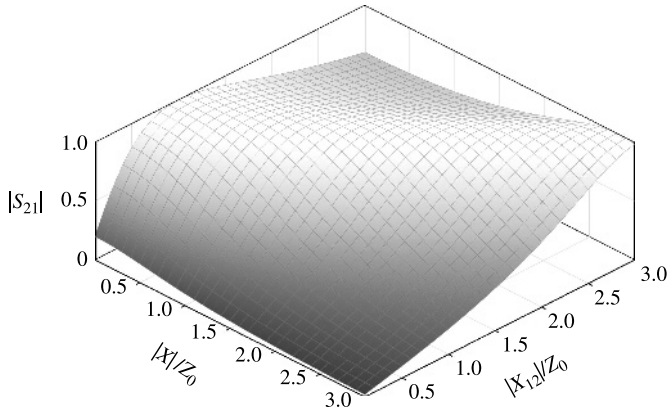

FIGURE 1.16 Plot of the modulus of the transmission coefficient $t = S_{21}$ (1.57) as a function of the modulus of the reactances $X_{11} = X_{22} = X$ and X_{21} (*Source*: Reprinted with permission from [63]; copyright 2005 by the American Physical Society.)

placed at the theoretical location of the image (i.e., at a distance $2d$ from the source), the perfect lens behaves as a perfect tunneling (or perfect matching) device, giving a maximum of power transmission at the theoretical location of the image (i.e., at the point marked as S' in Fig. 1.14). If the antennas are not identical, but none can be considered a small probe (in the sense defined in the previous paragraph), the location and magnitude of the maximum transmission will vary. This tunneling effect in metamaterial perfect lenses and similar devices has been analyzed in detail in [63]. The experimental confirmation of such an effect has been shown in a device similar to Pendry's super-lens [73] (see also Chapter 5).

Two main conclusions arise from the above analysis. The first is that for field measurements at the back side of a metamaterial super-lens, care must be taken in order to avoid artifacts coming from the matching/tunneling capabilities of such devices. The second is that, in some circumstances, it may be possible to take advantage of such a tunneling effect in order to obtain additional information from the image. For instance, if the shape and characteristics of the source are known, it is possible to design an appropriate detector in order to determine the source location in three-dimensional space from measurements of the transmission coefficient behind the lens.

1.10 LOSSES AND DISPERSION

After the first seminal papers showing propagation in left-handed media, it was claimed that losses and dispersion will destroy many of the previously reported effects. Specifically, negative refraction [15] and super-resolution in Pendry's perfect lens [58] were criticized. The analysis of the refraction of a Gaussian beam at the interface between an ordinary and a left-handed medium showed, without doubt, that negative refraction occurs in such a situation [16,17], thus confirming the Veselago analysis [6]. Of more interest are the effects of losses on the perfect lens proposed by Pendry [26]. This effect was analyzed in [59–61] among others, leading to similar conclusions. In the following we will briefly examine this aspect.

In order to develop the analysis, it is convenient to rewrite the transmission coefficient (1.39) as

$$t = \frac{4Z}{(1+Z)^2 \exp(jk_{x,2}d) - (1-Z)^2 \exp(-jk_{x,2}d)}, \tag{1.58}$$

where $Z = Z_2/Z_1$. If $\varepsilon/\varepsilon_0 \to -1$ and $\mu/\mu_0 \to -1$, from our definitions of positive waves[6] and from equation (1.30), it follows that $Z = 1$ if $k_{x,2} = -|k_{x,2}|$ is real, and $Z = -1$ if $k_{x,2} = -j\alpha$ is imaginary. Therefore $t \to \exp(j|k_{x,2}|d)$ for propagative waves and $t \to \exp(\alpha d)$ for evanescent waves. In both cases, the phase and amplitude

[6]According to our definitions (see Fig. 1.7 as well as Section 1.7 and equation 1.12), in the left-handed slab, propagation is backward and positive waves are defined with $\mathrm{Re}(k_{x,2}) < 0$ and/or $\mathrm{Im}(k_{x,2}) < 0$. In ordinary media, positive waves are defined with $\mathrm{Re}(k_{x,2}) > 0$ and/or $\mathrm{Im}(k_{x,2}) < 0$, as usual.

of the incident waves change along the slab just by the amount necessary to produce Fourier harmonics restoration at a distance $2d$ from any source (see Section 1.9.3). Let us now introduce a small amount of losses in the left-handed slab, so that $\varepsilon \to -\varepsilon_0(1 + j\delta_\varepsilon)$ and $\mu \to -\mu_0(1 + j\delta_\mu)$. Let us also suppose that $k_z \gg k_0$, so that $k_{x,2} = -j\alpha \simeq -j|k_z|$. In such limit, taking into account equation (1.30), we obtain

$$t \to \frac{4}{4\ \exp(-|k_z|d) - \delta_\mu^2\ \exp(|k_z|d)}. \tag{1.59}$$

Therefore, for high values of k_z it is still $t \simeq \exp(|k_z|d) \simeq \exp(\alpha d)$ provided $\delta_\mu^2 \exp(|k_z|d) < 4\exp(-|k_z|d)$, or

$$|k_z|d \lesssim \ln\left(\frac{2}{\delta_\mu}\right). \tag{1.60}$$

However, if the above condition is not fulfilled, then $t \sim \exp(-|k_z|d)$, and evanescent waves are not amplified inside the left-handed slab. A similar (dual) result holds for *p*-polarized (or TM) modes.

Regarding the analysis of Section 1.9.3, the above results imply that, in general, a lossy left-handed slab with $\varepsilon/\varepsilon_0 \to -(1 + j\delta_\varepsilon)$ and $\mu/\mu_0 \to -(1 + j\delta_\mu)$ will *see* the effective source (1.53) with

$$k_{\max} \approx \frac{1}{d}\ln\left(\frac{2}{\delta}\right); \qquad \delta = \max\left(\delta_\varepsilon, \delta_\mu\right), \tag{1.61}$$

so that the source is *seen* at the image with a resolution Δ given by

$$\frac{\Delta}{d} \gtrsim \frac{2\pi}{k_{\max}d} = 2\pi\left\{\ln\left(\frac{2}{\delta}\right)\right\}^{-1}. \tag{1.62}$$

It is worth noting that the wavelength of the incident radiation does not appear in equation (1.62), only the losses and thickness limit the resolution of the device.

An interesting consequence of the above results is that losses prevent the divergence of energy mentioned in section 1.9.3. In fact, because Fourier harmonics are only restored upto some finite value of $|k_z| = k_{\max}$, the energy divergence associated with the harmonics in the limit $|k_z| \to \infty$ disappears. However, this regularization takes place at the cost of a loss in resolution. Thus, the lossy perfect lens is, in fact, a *super-lens*, with a resolution limited by equation (1.62). As the free-space wavelength is not present in equation (1.62), the resolution of such a lens may still overcome the diffraction limit ($\Delta \lesssim \lambda_0$). However, the logarithmic dependence on $1/\delta$ of Δ/d strongly limits this effect. In fact, even in the best dielectrics, δ_ε is not

much smaller than 10^{-3}. Therefore, as a consequence of equation (1.62), super-resolution can only be present in left-handed slabs with a width of only a fraction of the wavelength. Thus, in practice, any left-handed super-lens is a near-field device whose effectiveness should be measured with regard to other near-field microscopy devices [76]. In order to reduce the limitations caused by losses in the super-lens performance, multilayer lenses formed by alternating layers of ordinary and left-handed media have been proposed [77,78]. Such devices provide a larger distance between the source and the image, but not a larger distance between the source and the left interface of the lens.

The above analysis can easily be extended to variations in the real part of ε and μ: $\varepsilon \rightarrow -\varepsilon_0(1+\delta_\varepsilon)$ and $\mu \rightarrow -\mu_0(1+\delta_\mu)$ [59]. The results are quite similar to those reported in the previous paragraph. The main difference is that these small variations of ε or μ may allow for the excitation of slab guided waves (see Section 1.8.2) for some values of the transverse wavenumber. In such cases, very high values of the transmission coefficient are obtained for the corresponding spatial Fourier harmonic [59], which may distort the image. As left-handed metamaterials are highly dispersive media, this effect may appear for sources emitting radiation pulses of finite duration.

The effect of the finite duration of RF pulses in the focusing of rays in the Veselago lens was also analyzed in [61]. The main conclusion is that, for the effective focusing of a ray, the pulse duration should be longer than the time taken by light to travel between the source and the focus along such a ray.

1.11 INDEFINITE MEDIA

Upto now, we have focused our attention on isotropic left-handed media. However, most present realizations of such media are in fact highly anisotropic, showing a left-handed behavior only for very specific polarizations and directions of propagation. These structures (some of them will be described in detail in the following chapters of this book) are easier to manufacture than isotropic left-handed media, while keeping many of their interesting properties. Therefore, they are of great practical interest. Many of them can be described by means of symmetric and simultaneously diagonalizable permittivity, $\overline{\overline{\varepsilon}}$, and permeability, $\overline{\overline{\mu}}$, tensors with some negative eigenvalues. These media have been called *indefinite* media [53], a denomination that emphasizes that not all the eigenvalues of the constitutive tensors have the same sign. In this section, wave propagation in indefinite media will be briefly discussed. This discussion will mainly follow the analysis in [53].

In order to simplify the analysis, we will choose a system of reference such that both $\overline{\overline{\varepsilon}}$ and $\overline{\overline{\mu}}$ are diagonal:

$$\overline{\overline{\varepsilon}} = \begin{pmatrix} \varepsilon_x & 0 & 0 \\ 0 & \varepsilon_y & 0 \\ 0 & 0 & \varepsilon_z \end{pmatrix}; \qquad \overline{\overline{\mu}} = \begin{pmatrix} \mu_x & 0 & 0 \\ 0 & \mu_y & 0 \\ 0 & 0 & \mu_z \end{pmatrix}. \tag{1.63}$$

Because the dispersion relation for plane waves of generic polarization propagating in such a medium may be rather complicated, we will focus our attention on some particular cases of interest. In particular we will consider the very important case of TE waves polarized along a main axis of $\overline{\overline{\varepsilon}}$ and $\overline{\overline{\mu}}$. As in the previous sections we will choose, without loss of generality, $\mathbf{E} = E\,\hat{\mathbf{y}}$. The dispersion relation for such waves is [53]

$$\omega^2 = \frac{k_z^2}{\varepsilon_y \mu_x} + \frac{k_x^2}{\varepsilon_y \mu_z} \tag{1.64}$$

(the dispersion relation for TM waves is the dual one). Taking ω as a parameter, equation (1.64) defines the isofrequency curves in the (k_z, k_x) plane. These curves may be ellipses or hyperbolae, depending on the signs of $\varepsilon_y \mu_x$ and $\varepsilon_y \mu_z$. It may be worth mentioning that, because left-handed media are highly dispersive, the constitutive parameters in equations (1.63) and (1.64) are usually frequency dependent. Therefore, in practical indefinite media, the shape of these curves may change from hyperbolic to elliptic, and vice versa, depending on frequency.

The direction of propagation of optical rays and energy is defined by the group velocity $\mathbf{v}_\mathrm{g} = \nabla_\mathbf{k}\omega(\mathbf{k})$. From equation (1.64) it is readily found that

$$\mathbf{v}_\mathrm{g} = \frac{1}{\omega}\left(\frac{k_x}{\varepsilon_y \mu_z}, 0, \frac{k_z}{\varepsilon_y \mu_x}\right). \tag{1.65}$$

The angle between group and phase ($\mathbf{v}_\mathrm{p} = \mathbf{k}\omega/k^2$) velocities is defined by

$$\mathbf{v}_\mathrm{p} \cdot \mathbf{v}_\mathrm{g} = \frac{1}{k^2}\left(\frac{k_x^2}{\varepsilon_y \mu_z} + \frac{k_z^2}{\varepsilon_y \mu_x}\right), \tag{1.66}$$

which generalizes equation (1.18). The laws for the refraction of optical rays at the interface of an indefinite media can be deduced from equation (1.64) by imposing the continuity of the tangential component of the wavevector $\mathbf{k}$ at the interface, and using equation (1.66) to draw the rays in the indefinite media [24] (see Fig. 1.4 and Problem 1.8). Equation (1.64) is also useful for analyzing the propagation of TE modes in rectangular waveguides filled with indefinite media [79], or the amplification of TE evanescent modes by slabs made of such media [53].

PROBLEMS

1.1. Quasistatic plasmonic resonance of a sphere. Find the polarization of a sphere of permeability $\varepsilon < 0$ in the presence of a uniform quasielectrostatic field. Assume a plasmonic type of frequency dependence $\varepsilon = \varepsilon_0(1 - \omega_\mathrm{p}^2/\omega^2)$, and find the frequency of oscillation of quasistatic polarization modes.

1.2. Quasistatic surface plasmons. Show that Laplace's equation at the interface between two media, 1 and 2, has bounded propagative solutions along such interface provided $\varepsilon_1 = -\varepsilon_2$. These solutions are usually called quasistatic surface plasmons [3].

1.3. Full-wave surface plasmons–polaritons. Find the dispersion relation for TM surface waves at the interface between two media with $\varepsilon_1 > 0$ and $\varepsilon_2 < 0$. Show that these solutions converge to the aforementioned surface plasmons (see Problem 1.2) in the limit $k \to \infty$. For small values of k, these waves have a different dispersion relation and are sometimes called *surface polaritons*. See [3] for a deeper discussion on surface plasmons–polaritons.

1.4. Energy flow of a plane wave in a left-handed medium. Show that equation (1.14) ensures that the density of energy (U) and the energy flux (the Poynting vector $\mathbf{S}$) of a plane wave in a lossless left-handed medium are related through $\mathbf{S} = \mathbf{v}_g U$.

1.5. Left-handed concave and convex lenses. Show that a concave (convex) lens made of a left-handed metamaterial becomes convergent (divergent). These lenses were analyzed in [6].

1.6. Refraction of nonparaxial rays by a left-handed slab. Study the refraction of nonparaxial rays coming from a point source by a left-handed slab, and find the distance from the source at which these rays refocus. Show that this distance reduces to equation (1.22) for paraxial rays.

1.7. Dispersion relation for p-polarized surface waves. Find the dispersion relation for p-polarized (or TM, or LSM) surfaces waves at the interface between a left-handed medium and free space. Show that it is deduced from equation (1.37) by the duality transformations $\varepsilon \to \mu$, $\mu \to \varepsilon$, $\mathbf{E} \to \mathbf{H}$, $\mathbf{H} \to -\mathbf{E}$ (see [14]).

1.8. All-angle negative refraction by an indefinite uniaxial dielectric. Study the refraction of plane waves at the interface between free space and a uniaxial dielectric with $\mu = \mu_0$, $\varepsilon_\parallel < 0$ and $\varepsilon_\perp = \varepsilon_0$. Show that *all-angle negative refraction* occurs for p-polarized (TM) waves when the optical axis is perpendicular to the interface. Similar systems have been analyzed in [9,24].

1.9. Energy flow in surface waves. Show that in the surface waves (1.37), power flows in the backward direction inside the left-handed material, and in the forward direction in free space. Discuss, in terms of the constitutive parameters, if the whole surface wave is forward or backward.

1.10. Small resonators made with left-handed media. Study the resonant modes of a one-dimensional cavity made of two consecutive slabs of ordinary and left-handed media, placed between two parallel metallic plates. Show that the condition for the resonance of TEM waves does not depend on the distance between the plates, but on the relative width of the slabs. This and other similar resonators and waveguides have been proposed in [47].

1.11. Modes in parallel-plate waveguides partially filled by a left-handed slab. Find, making use of the transverse transmission matrix technique, the dispersion relation for TE and TM modes in parallel plate waveguides partially filled by a left-handed slab. This and other similar waveguides have been analyzed in [38].

1.12. Phase compensation in single negative slabs. Show that all-angle phase compensation and amplification of evanescent waves also occurs in two consecutive slabs with $0 < \varepsilon_2 = -\varepsilon_1$ and $0 > \mu_2 = -\mu_1$, provided the widths of both slabs are identical. Draw a plot of the amplitude of electromagnetic waves inside this system for the different aforementioned effects. See [52] for a deeper discussion on the properties of a pair of consecutive single negative slabs.

1.13. Asymmetric perfect lens. Find the transmission coefficient through a left-handed slab with $\varepsilon = -\varepsilon_0$ and $\mu = -\mu_0$ sandwiched between free space and a semi-infinite medium with $0 < \varepsilon \neq \varepsilon_0$ and $0 < \mu \neq \mu_0$. This system is sometimes called an asymmetric perfect lens [67].

1.14. Near-field near-perfect lens made with a medium with $\varepsilon = -\varepsilon_0$. Find the transmission coefficient for evanescent quasielectrostatic waves (i.e., solutions to Laplace's equation of the kind $\phi(\mathbf{r}) = \phi_0 \exp(-j\mathbf{k} \cdot \mathbf{r})$) through a slab with $\varepsilon = -\varepsilon_0$ and $\mu = \mu_0$. Show that this slab behaves as a near-field near-perfect lens for the quasielectrostatic field. A deeper discussion of this proposal can be found in [26] and in [68–71], among others.

1.15. TE anticutoff waveguide made with an indefinite uniaxial medium. Find the dispersion relation for the fundamental $TE_{1,0}$ mode in a rectangular waveguide filled with a uniaxial indefinite medium with $\varepsilon = \varepsilon_0$, $\mu_x = \mu_y = \mu_0$, $\mu_z < 0$ (see Fig. 1.9 for the axis definition). Show that this mode has an anticutoff behavior; that is, it is propagative below certain cutoff frequency and evanescent above this frequency. This device has been studied and experimentally demonstrated in [79].

1.16. TM anticutoff waveguide made with an indefinite uniaxial medium. Find the dispersion relation for the fundamental $TM_{1,1}$ mode in a rectangular waveguide filled with a uniaxial indefinite medium with $\mu = \mu_0$, $\varepsilon_x = \varepsilon_0$, $\varepsilon_y = \varepsilon_z < 0$ (see Fig. 1.9 for the axis definition). Show that this mode has an anticutoff behavior; that is, it is propagative below a certain cutoff frequency and evanescent above this frequency. This device has been studied and experimentally demonstrated in [80].

REFERENCES

1. J. D. Jackson *Classical Electrodynamics*. Wiley, New York, 1999 (3rd ed.).
2. L. D. Landau, E. M. Lifshitz, and L. P. Pitaevskii *Electrodynamics of Continuous Media*. Pergamon, New York, 1984.

3. H. Raether *Excitation of Plasmons and Interband Transitions by Electrons*. Springer, Berlin, 1980.
4. M. S. Sodha and N. C. Shrivastava *Microwave Propagation in Ferrimagnetics*. Plenum Press, New York, 1981.
5. A. G. Gurevich and G. A. Melkov *Magnetization Oscillations and Waves*. CRC Press, Boca Raton, Florida, 1996.
6. V. G. Veselago "The electrodynamics of substances with simultaneously negative values of ε and μ." *Sov. Phys. Usp.*, vol. 47, pp. 509–514, 1968.
7. D. R. Smith, W. J. Padilla, D. C. Vier, S. C. Nemat-Nasser, and S. Schultz "Composite medium with simultaneously negative permeability and permittivity." *Phys. Rev. Lett.*, vol. 84, pp. 4184–4187, 2000.
8. V. G. Veselago "Formulating Fermat's principle for light travelling in negative refraction materials." *Physics–Uspekhi*, vol. 45, pp. 1097–1099, 2002.
9. I. V. Lindell, S. A. Tretyakov, K. I. Nikoskinen, and S. Ilvonen "BW-media with negative parameters, capable of supporting backward waves." *Microwave Opt. Tech. Lett.*, vol. 31, pp. 129–133, 2001.
10. R. W. Ziolkowski and E. Heynman "Wave propagation in media having negative permeability and permittivity." *Phys. Rev. E*, vol. 64, paper 056625, 2001.
11. A. Sihvola "Electromagnetic emergence in metamaterials." In *Advances in Electromagnetics of Complex Media and Metamaterials*, S. Zouhdi, A. Sihvola, M. Arsalane Eds., NATO Science Series: II: Mathematics, Physics, and Chemistry, vol. 89, pp. 1–17, Kluwer Academic Publishers, Dordrecht, 2003.
12. S. Ramo, J. R. Whinnery, and T. Van-Duzer *Fields and Waves in Communication Electronics.* John Wiley, New York, 1965.
13. M. Mrozowski *Guided Electromagnetic Waves. Properties and Analysis.* Research Studies Press (Taunton, UK) and John Wiley (New York), 1997.
14. R. F. Harrington *Time-harmonic Electromagnetic Fields.* McGraw-Hill, New York, 1961.
15. P. M. Valanju, R. M. Walser, and A. P. Valanju "Wave refraction in negative-index media: Always positive and very inhomogeneous." *Phys. Rev. Lett.*, vol. 88, paper 187401, 2002.
16. D. R. Smith, D. Schurig, and J. B. Pendry "Negative refraction of modulated electromagnetic waves." *Appl. Phys. Lett.*, vol. 81, pp. 2713–2715, 2002.
17. S. Foteinopoulou, E. N. Economou, and C. M. Soukoulis "Refraction in media with a negative refractive index." *Phys. Rev. Lett.*, vol. 90, paper 107402, 2003.
18. R. A. Shelby, D. R. Smith, and S. Schultz "Experimental verification of a negative index of refraction." *Science*, vol. 292, pp. 77–79, 2001.
19. C. G. Parazzoli, R. B. McGregor, K. Li, B. E. C. Kontenbah, and M. Tlienian "Experimental verification and simulation of negative index of refraction using Snell's law." *Phys. Rev. Lett.*, vol. 90, paper 107401, 2003.
20. K. Li, S. J. McLean, R. B. Gregor, C. G. Parazzoli, and M. H. Tanielian "Free-space focused-beam characterization of left-handed materials." *Appl. Phys. Lett.*, vol. 82, pp. 2535–2537, 2003.
21. A. A. Houck, J. B. Brock, and I. L. Chuang "Experimental observations of a left-handed material that obeys Snell's law." *Phys. Rev. Lett.*, vol. 90, paper 137401, 2003.

22. D. Felbacq and A. Moreau, "Direct evidence of negative refraction at media with negative ε and μ." *J. Opt. A: Pure and Appl. Opt.*, vol. 5, pp. L9–L11, 2003.
23. C. Luo, S. G. Johnson, and J. B. Pendry "All-angle negative refraction without negative effective index." *Phys. Rev. B*, vol. 65, 201104(R), 2002.
24. T. Gregorczyk, M. Nikku, X. Chen, B.-I. Wu, and J. A. Kong "Refraction laws for anisotropic media and their application to left-handed metamaterials." *IEEE Trans. Microwave Theory Tech.*, vol. 53, pp. 1443–1450, 2005.
25. M. Notomi "Theory of light propagation in strongly modulated photonic crystals: Refractionlike behavior in the vicinity of the photonic band gap." *Phys. Rev. B*, vol. 62, pp. 10696–10705, 2000.
26. J. B. Pendry "Negative refraction makes perfect lens." *Phys. Rev. Lett.*, vol. 85, pp. 3966–3969, 2000.
27. J. Lu, T. M. Gregorczyc, Y. Zhang, J. Pacheco, B. Wu, J. A. Kong, and M. Chen "Cerenkov radiation in materials with negative permittivity and permeability." *Opt. Express*, vol. 11, pp. 723–734, 2003.
28. K. Artmann "Berechnung der Seitenversetzung des totatreflektierten strahles." *Ann. Phys. Lpz.*, vol. 2, pp. 87–102, 1948.
29. J. A. Kong, B. I. Wu, and Y. Zhang "Lateral displacement of a Gaussian beam reflected from a grounded slab with negative permittivity and permeability." *Appl. Phys. Lett.*, vol. 80 pp. 2084–2086, 2002.
30. P. R. Bermann "Goos-Hänchen shift in negative refractive media." *Phys. Rev. E*, vol. 66, paper 067603, 2002.
31. R. W. Ziolkowski "Pulsed and CW Gaussian beam interactions with double negative metamaterial slabs." *Opt. Express*, vol. 11, pp. 662–681, 2003.
32. A. Lakhtakia "On planewave remittances and Goos-Hänchen shifts of planar slabs with negative real permittivity and permeability." *Electromagnetics*, vol. 23, pp. 71–75, 2002.
33. I. V. Shadrivov, A. A. Zharov, and Y. S. Kivshar "Giant Goos-Hänchen effect at the refraction from left-handed metamaterials." *Appl. Phys. Lett.*, vol. 83, pp. 2713–2715, 2003.
34. R. E. Collin *Field Theory of Guided Waves*. IEEE Press, New York, 1990 (2nd. ed.).
35. R. Ruppin "Surface polaritons of a left-handed medium." *Phys. Lett. A*, vol. 277, pp. 61–64, 2000.
36. S. A. Darmanyan, M. Neviere, and A. A. Zakhidov "Surface modes at the interface of conventional and left-handed media." *Opt. Commun.*, vol. 225, pp. 233–240, 2003.
37. R. Ruppin "Surface polaritons of a left-handed material slab." *J. Phys.: Cond. Matter*, vol. 13, pp. 1811–1818, 2001.
38. A. Alu and N. Engheta "Guided modes in a waveguide filled with a pair of single negative (SNG), double negative (DNG), and/or double positive (DPS) layers." *IEEE Trans. Microwave Theory Tech.*, vol. 52, pp. 199–210, 2004.
39. H. Coryand A. Burger "Surface-wave propagation along a metamaterial slab." *Microwave Opt. Tech. Lett.*, vol. 38, pp. 392–395, 2003.
40. B.-I. Wu, T. M. Gregorczyk, Y. Zhang, and J. A. Kong "Guided modes with imaginary transverse wave-number in a slab waveguide with negative permittivity and permeability." *J. Appl. Phys.*, vol. 93, pp. 9386–9388, 2003.

41. I. W. Shadrivov, A. A. Sukhorukov, and Y. S. Kivshar "Guided waves in negative refractive index waveguides." *Phys. Rev. E*, vol. 67, paper 057602, 2003.
42. I. S. Nefedov and S. A. Tretyakov "Waveguide containing a backward-wave slab." *Radio Sci.*, vol. 38, pp. 1101–1109, 2003.
43. P. Baccarelli, P. Burghignoli, F. Frezza, A. Galli, P. Lampariello, G. Lovat, and S. Paulotto "Fundamental modal properties of surface waves on metamaterial grounded slabs." *IEEE Trans. Microwave Theory Tech.*, vol. 53, pp. 1431–1442, 2005.
44. R. Ruppin "Extinction properties of a sphere with negative permittivity and permeability." *Solid State Commun.*, vol. 116, pp. 411–415, 2000.
45. V. Kuzmiak and A. A. Maradudin "Scattering properties of a cylinder fabricated from a left-handed material." *Phys. Rev. B*, vol. 66, paper 045116, 2002.
46. R. Ruppin "Surface polaritons and extinction properties of a left-handed material cylinder." *J. Phys.: Cond. Matter*, vol. 16, pp. 5991–5998, 2004.
47. N. Engheta and R. W. Ziolkowski "A positive future for double-negative metamaterials." *IEEE Trans. Microwave Theory Tech.*, vol. 53, pp. 1535–1556, 2005.
48. P. Bacarelli, P. Burghignoli, F. Frezza, A. Galli, P. Lampariello, G. Lovat, and S. Paulotto "Effects of leaky-wave propagation in metamaterial grounded slabs excited by a dipole source." *IEEE Trans. Microwave Theory Tech.*, vol. 53, pp. 32–44, 2005.
49. T. Tamir and A. A. Oliner "Guided complex waves. Part I: Fileds at an interface. Part II: Relation to radiation patterns." *Proc. Inst. Elec. Eng.*, vol. 110, pp. 310–334, 1963.
50. A. Grbic and G. Eleftheriades "Experimental verification of backward-wave radiation from a negative refractive index metamaterial." *J. Appl. Phys.*, vol. 92, pp. 5930–5935, 2002.
51. D. R. Fedkin and A. Ron "Effective left-handed (negative index) composite material." *Appl. Phys. Lett.*, vol. 81, pp. 1753–1755, 2002.
52. A. Alu and N. Engheta "Pairing an epsilon-negative slab with a mu-negative slab: resonance, tunneling and transparency." *IEEE Trans. Antennas Propag.*, vol. 51, pp. 2558–2571, 2003.
53. D. R. Smith and D. Schurig "Electromagnetic wave propagation in media with indefinite permittivity and permeability tensors." *Phys. Rev. Lett.*, vol. 90, paper 077405, 2003.
54. S. Maslowski, S. Tretyakov, and P. Alitalo "Near-field enhancement and imaging in double planar polariton-resonant structures." *J. Appl. Phys.*, vol. 96, pp. 1293–1300, 2004.
55. J. B. Pendry and S. A. Ramakrishna "Focusing light using negative refraction." *J. Phys.: Cond. Matter*, vol. 15, pp. 6345–6364, 2003.
56. J. D. Baena, L. Jelinek, R. Marqués, and F. Medina "Near-perfect tunneling and amplification of evanescent electromagnetic waves in a waveguide filled by a metamaterial: Theory and experiments." *Phys. Rev. B*, vol. 72, paper 075116, 2005.
57. Z. M. Zhang and C. J. Fu "Unusual photon tunneling in the presence of a layer with a negative refractive index." *Appl. Phys. Lett.*, vol. 80, pp. 1097–1099, 2002.
58. N. Garcia and M. Nieto-Vesperinas "Left-handed materials do not make perfect lens." *Phys. Rev. Lett.*, vol. 88, paper 207403, 2002.
59. D. R. Smith, D. Schurig, M. Rosenbluth, and S. Schultz "Limitations on subdiffraction imaging with a negative refractive index slab." *Appl. Phys. Lett.*, vol. 82, pp. 1506–1508, 2003.
60. R. Merlin "Analytical solution of the almost-perfect-lens problem." *Appl. Phys. Lett.*, vol. 84, pp. 1290–1292, 2004.

61. R. Marques and J. Baena "Effect of losses and dispersion on the focusing properties of left-handed media." *Microwave Opt. Tech. Lett.*, vol. 41, pp. 290–294, 2004.
62. G. Tayeb and S. Enoch "Perfect lenses made with left-handed materials: Alices mirror?" *J. Opt. Soc. Am.*, vol. 21, pp. 1417–1423, 2004.
63. F. Mesa, R. Marques, M. Freire, and J. D. Baena "Three dimensional super-resolution in metamaterial slab lenses." *Phys. Rev. B*, vol. 72, paper 235117, 2005.
64. A. Grbic and G. Eleftheriades "Overcoming diffraction limit with a planar left-handed transmission line lens." *Phys. Rev. Lett.*, vol. 92, paper 117403, 2004.
65. J. M. Williams "Some problems with negative refraction." *Phys. Rev. Lett.*, vol. 87, paper 249703, 2001.
66. V. G. Veselago "Some remarks regarding electrodynamics of materials with negative refraction." *Appl. Phys. B*, vol. 81, pp. 403–407, 2005.
67. S. A. Ramakrishna, J. B. Pendry, D. R. Smith, D. Schurig, and S. Schultz "The asymmetric lossy near-perfect lens." *J. Mod. Opt.*, vol. 49, pp. 1747–1762, 2002.
68. J. T. Shen and P. M. Platzman "Near field imaging with negative dielectric constant lenses." *Appl. Phys. Lett.*, vol. 80, pp. 3286–3288, 2002.
69. N. Fang and X. Zhang "Imaging properties of a metamaterial superlens." *Appl. Phys. Lett.*, pp. 161–163, 2003.
70. N. Fang, H. Lee, C. Sun, and X. Zhang "Sub-diffraction-limited optical imaging with a silver superlens." *Science*, vol. 308, pp. 534–537, 2005.
71. R. J. Blaikie and D. O. S. Melville "Imaging through planar silver lenses in the optical near field." *J. Opt. A*, vol. 7, pp. S176–S183, 2005.
72. R. Marques, F. Mesa, and F. Medina "Near-field enhanced imaging by a metamaterial magnetized ferrite slab." *Appl. Phys. Lett.*, vol. 86, paper 023505, 2005.
73. M. J. Freire and R. Marques "Planar magnetoinductive lens for three dimensional subwavelength imaging." *Appl. Phys. Lett.*, vol. 86, paper 183505, 2005.
74. V. Veselago "Superlens as a matching device." http://xxx.lanl.gov/ftp/cond-mat/papers/0501/0501438.pdf
75. D. M. Pozar *Microwave Engineering* Addison-Wesley, Reading, MA, 1993.
76. M. Nieto-Vesperinas "Problem of image superresolution with a negative—refractive—index slab." *J. Opt. Soc. Am. A*, vol. 21, pp. 491–498, 2004.
77. E. Shamonina, V. A. Kalinin, K. H. Ringhofer, and L. Solymar "Imaging, compression and Poynting vector streamlines with negative permittivity materials." *Electron. Lett.*, vol. 37, pp. 1243–1244, 2001.
78. S. A. Ramakrishna, J. B. Pendry, M. C. K. Wiltshire, and W. J. Stewart "Imaging the near field." *J. Mod. Opt.*, vol. 50, pp. 1419–1430, 2003.
79. S. Hrabar, J. Bartolic, and Z. Sipus "Waveguide miniaturization using uniaxial negative permeability metamaterial." *IEEE Trans. Antennas Propag.*, vol. 53, pp. 110–119, 2005.
80. J. Esteban, C. Camacho-Peñalosa, J. E. Page, T. M. Martin-Guerrero, and E. Marquez-Segura "Simulation of negative permittivity and negative permeability by means of evanescent waveguide modes–theory and experiment." *IEEE Trans. Microwave Theory Tech.*, vol. 53, pp. 1506–1514, 2005.